



**HAL**  
open science

## Assessment of the relative impacts of climate changes and anthropogenic forcing on spring discharge of a Mediterranean karst system

Vianney Sivelles, Hervé Jourde, Daniel Bittner, Naomi Mazzilli, Yves Trambly

### ► To cite this version:

Vianney Sivelles, Hervé Jourde, Daniel Bittner, Naomi Mazzilli, Yves Trambly. Assessment of the relative impacts of climate changes and anthropogenic forcing on spring discharge of a Mediterranean karst system. *Journal of Hydrology*, 2021, 598, pp.126396. 10.1016/j.jhydrol.2021.126396 . hal-03216522

**HAL Id: hal-03216522**

**<https://hal.science/hal-03216522>**

Submitted on 24 May 2023

**HAL** is a multi-disciplinary open access archive for the deposit and dissemination of scientific research documents, whether they are published or not. The documents may come from teaching and research institutions in France or abroad, or from public or private research centers.

L'archive ouverte pluridisciplinaire **HAL**, est destinée au dépôt et à la diffusion de documents scientifiques de niveau recherche, publiés ou non, émanant des établissements d'enseignement et de recherche français ou étrangers, des laboratoires publics ou privés.



Distributed under a Creative Commons Attribution - NonCommercial 4.0 International License

# 1 Assessment of the relative impacts of climate 2 changes and anthropogenic forcing on spring 3 discharge of a Mediterranean karst system

4 Vianney Sivelles <sup>1\*</sup>, Hervé Jourde <sup>1</sup>, Daniel Bittner <sup>2,3</sup>, Naomi Mazzilli <sup>4</sup>, and Yves Trambly <sup>1</sup>

5 <sup>1</sup> HydroSciences Montpellier (HSM), Université de Montpellier, CNRS, IRD, 34090 Montpellier,  
6 France

7 <sup>2</sup> Faculty of Civil, Geo and Environmental Engineering, Technical University of Munich, Arcisstr. 21,  
8 80333, Munich, Germany

9 <sup>3</sup> Erftverband, Department for River Basin Management, Am Erftverband 6, 50126 Bergheim, Germany

10 <sup>4</sup> EMMAH, INRAE, Avignon Université, 84000, Avignon, France

11 \* corresponding author: HydroSciences Montpellier, 3000 avenue Emile Jeanbrau, 34090 Montpellier  
12 (France) - vianney.sivelles@umontpellier.fr

13

## 14 Highlights

- 15
- 16 • Multiple climate change and groundwater abstraction scenario testing procedure for future  
development of karst spring discharge.
  - 17 • Climate change has a major effect on the future evolution of spring discharge.
  - 18 • Groundwater abstraction constitutes a secondary factor in the spring dry-up.
  - 19 • The aquifer is not overexploited yet but still highly sensible to groundwater extraction.
- 20

## 21 Abstract

22 The Mediterranean region is a climate change hotspot where the rate of climate change exceeds the  
23 global mean. The rapidly changing climate in combination with an increase in anthropogenic pressures  
24 cause water resources in the Mediterranean basin to become increasingly scarce. Modelling future water  
25 resource availability considering both climate and anthropogenic changes on karst catchments remains  
26 a major challenge in the field of hydrology. The purpose of this study is to assess the relative effects of  
27 climate change and anthropogenic forcing on the spring discharge of a Mediterranean karst system by  
28 coupling 12 climate model simulations under two emission scenarios (RCP 4.5 and RCP 8.5) with three  
29 hydrological models and four scenarios of future groundwater extraction for drinking water supply (no  
30 abstraction, present-day abstraction, +50% abstraction and +100% abstraction at horizon 2100). The  
31 study area is the Oeillal spring's karst catchment which is located at the Fonfroide-Monredon massif  
32 located in Southern France. The periods of spring drying-up can increase up to 30% according the RCP

33 4.5 and up to 70% according the RCP 8.5. This may be aggravated by groundwater abstraction in the  
34 area which, combined with climate change, could contribute to double the length of spring drying-up  
35 period in the worst scenario. The main results of the study suggest that climate change has a major effect  
36 on the future evolution of the Oeillal spring's discharge and that groundwater abstraction constitutes a  
37 secondary but non-negligible factor which increases the occurrence of drying-up of this Mediterranean  
38 spring.

39 **Keywords**

40 Climate change, Mediterranean karst aquifer, Lumped parameters model, Karst hydrology

## 41 **1 Introduction**

42 The Mediterranean basin strongly depends on water from karst aquifers. It is estimated that at least one-  
43 quarter of the domestic water in the Mediterranean basin comes from karst aquifer resources  
44 (Bakalowicz, 2015). Large areas in the Mediterranean basin are shaped by carbonate rock outcrops in  
45 i.e. Montenegro (80.1%), Bosnia and Herzegovina (60.5%), Slovenia (49.5%), Croatia (40.9 %), France  
46 (35.0%) (Goldscheider et al., 2020; Stevanović, 2018). Ensuring a sustainable karst freshwater supply  
47 in the area thus constitutes a major challenge considering climate change impacts and future  
48 anthropogenic pressures, including an increase in water abstraction or changes in land cover and land-  
49 use (LCLU), both of which may have a strong impact on future availability of karst water resources  
50 (Gleeson et al., 2012; Taylor et al., 2013).

51 The Mediterranean region has been identified to be particularly vulnerable to climate change, where  
52 future scenarios indicate a decrease of precipitation together with an increase in temperature  
53 (Diffenbaugh and Giorgi, 2012; Giorgi, 2006). In the South of France, for example, changes in the mean  
54 annual temperature have been observed since the late 1970s (Lelièvre et al., 2010). The recorded  
55 warming in the area was about +0.49 °C/decade for the period of 1979-2004 (Lespinas et al., 2010)  
56 wherefore the value is significantly higher than the global average estimated to be about +0.27°C/decade  
57 within the same period (Brohan et al., 2006). The combination of temperature and precipitation changes  
58 will have strong impacts on the soil water content available for evapotranspiration (Lavorel et al., 1998)  
59 causing recharge processes to change (Tramblay et al., 2020). Moreover, population developments in  
60 the Mediterranean region will further amplify the water stress caused by climate change (Stefano et al.,  
61 2012; Vörösmarty et al., 2000). Thus, it is important to assess the combined potential impacts of climate  
62 change and anthropogenic pressures in the Mediterranean basin, particularly considering that water  
63 resources are already affected by environmental changes, such as climate evolution and LCLU changes  
64 (García-Ruiz et al., 2011).

65 The effects of climate change on karst springs in the Mediterranean have already been investigated.  
66 Nerantzaki and Nikolaidis (2020) observed an increased dryness in terms of frequency, duration and  
67 intensity for three Mediterranean karst springs located in Greece. Smiateck et al. (2013) highlighted a

68 reduction of 9% and 30% of the annual discharge of the Figeih spring in Syria by the middle and the end  
69 of the 21<sup>st</sup> century respectively. Doummar et al. (2018) identified the effect of climate change on the  
70 Assal spring in Lebanon, where the discharge could decrease up to 50% after 2070. Dubois et al. (2020)  
71 estimated that a 30% reduction of rainfall induces a loss of 36% of the discharge of the Qachqouch  
72 spring in Lebanon which leads to water shortages that last longer and occur earlier in the season. A  
73 similar trend was observed for a karst system located in Southern Italy (Fiorillo and Guadagno, 2012).  
74 In Palestine, Hartmann et al. (2012) show that the discharge of the Faria spring will decrease by 30%  
75 by the end of the 21<sup>st</sup> century. According to the authors, the main reason for this development was not  
76 climate change but the uncontrolled pumping and drilling activities in the area. The impacts of  
77 groundwater abstraction on Mediterranean karst systems under active management (i.e. the pumping  
78 rate is set to mobilize the aquifer's stored reserve) has also been subject to various studies (Charlier et  
79 al., 2015; Jourde et al., 2014; Ladouche et al., 2014). Nonetheless, there is a lack of knowledge regarding  
80 the combined potential impacts of anthropogenic forcing and climate change at the catchment scale as  
81 it has until to date only been investigated on large scales (Wada et al., 2016).

82 Assessing climate change and anthropogenic impacts on hydrological processes in karst systems often  
83 relies on the use of hydrological models (Hartmann et al., 2012; Nerantzaki and Nikolaidis, 2020; Sapač  
84 et al., 2019). Various types of hydrological models can be implemented in karst studies, all based on  
85 different conceptual approaches. One common approach is to consider different combinations of the  
86 dominant flow compartment as distinct buckets (Chang et al., 2017; Fleury et al., 2007; Guinot et al.,  
87 2015; Mazzilli et al., 2019). Most of the frequently used lumped-parameters model in karst hydrology  
88 consider homogeneous recharge processes at the catchment scale. Depending on land-use,  
89 heterogeneities in soil properties, heterogeneities in climate inputs (e.g. convective events, altitudinal  
90 gradient), and catchment size, it can be of interest to consider a pseudo-distributed recharge (Bittner et  
91 al., 2018; Hartmann et al., 2012; Ollivier et al., 2020). However, making reliable predictions of climate  
92 change and anthropogenic pressures like land-use change impacts on karst systems remains a major  
93 challenge for hydrological models (Devia et al., 2015) due to the conceptualization as well as parametric  
94 uncertainties (Perrin et al., 2001; Refsgaard and Henriksen, 2004). Therefore, most studies dealing with

95 the assessment of climate change and anthropogenic impacts on karst systems either consider multi-  
96 model approaches (Hartmann et al., 2012; Jiang et al., 2007; Jones et al., 2006) or verify the conceptual  
97 and parametric transferability of a model to other catchments (Bittner et al., 2018) to limit the bias  
98 induced by the uncertainties on conceptualization and parameterization. The literature research  
99 conducted within this study yielded several studies that either focus on climate change impacts (Klaas  
100 et al., 2020; Loáiciga et al., 2000; Nerantzaki and Nikolaidis, 2020; Sapač et al., 2019; Smiatek et al.,  
101 2013) or on anthropogenic impacts on karst spring discharge within the Mediterranean basin (Hartmann  
102 et al., 2012; Hartmann et al., 2014; Stevanovic, 2010; Stevanović, 2018). To the best of our knowledge,  
103 however, there is no study accounting for both, climate change and anthropogenic impacts on karst  
104 spring discharge.

105 The purpose of this study is to assess the relative impacts of climate change and anthropogenic activity  
106 on the future evolution of spring discharges of a Mediterranean karst system (Oeillal spring, Southern  
107 France). In this study, anthropogenic pressure results from increasing groundwater abstraction rates due  
108 to an increasing water demand. Using a suitable ensemble of climate change simulations and different  
109 pumping scenarios, the combined effects of climate change and anthropogenic forcing on groundwater  
110 resource dynamics can be investigated. To obtain reliable unbiased results, we considered a total of three  
111 different conceptual models. On all three models, all possible combinations of climate change  
112 projections and pumping scenarios were run, allowing us to assess the relative impact of climate change  
113 and anthropogenic pressures on the spring discharge of the studied Mediterranean karst system.

## 114 **2 Study area**

### 115 **2.1 Geological and hydrogeological settings**

116 The Oeillal spring's catchment is located in the Narbonne-Sigean sedimentary basin, composed of  
117 Oligocene sediments, alluvions from the Aude river and limestone terrains of the Fonfroide-Monredon  
118 massif (Figure 1). The main aquifer in the area runs within the calcareous formation and fed the Oeillal  
119 spring, which is located in the Western part of the Narbonne-Sigean sedimentary basin and rises at four

120 spring pools. In the Northern part of the area, there is also an alluvial aquifer which is contained in the  
 121 Quaternary formation of the Aude river's terrace.

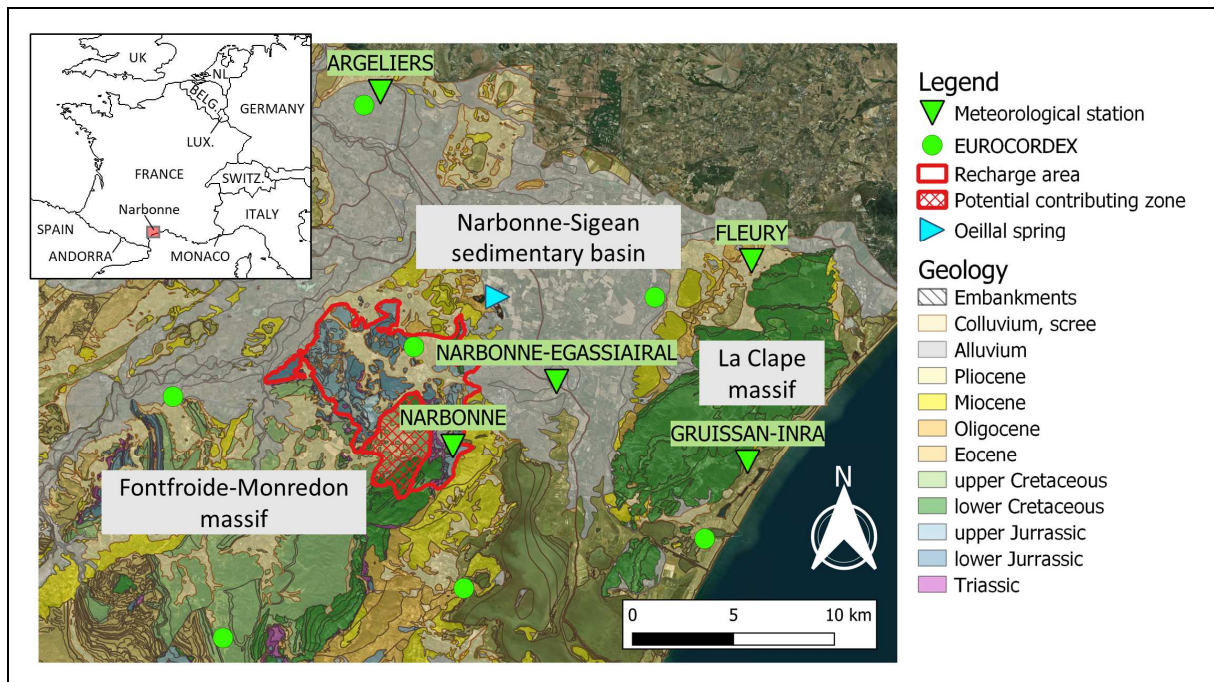


**Figure 1: Geological setting, meteorological monitoring (Météo-France) and climate simulation grid (EURO-CORDEX) of the study area.**

122 The geological formations of the basin were primarily formed during the Oligocene when significant  
 123 rifting occurred which simultaneously marked the beginning of the uplifting of the geological formations  
 124 of the Malvesi area. The presence of a normal fault causes the Jurassic unit to rise in the form of a horst,  
 125 called the Montlaures massif near the Oeillal spring (Figure 2). If no horst is formed, the Jurassic unit is  
 126 covered by Oligocene sediments which can be differentiated according to three different sedimentary  
 127 series: (1) the grey series during early Oligocene (lake deposit), (2) the transition series, and (3) the red  
 128 series (floodplain deposits and conglomerate channels). In the Jurassic unit, a higher piezometric level  
 129 can be detected which indicates a potential upward vertical leakage towards the Oligocene sediments.  
 130 Additionally, the Oligocene sediments may locally show higher permeabilities due to the presence of  
 131 either conglomerate, dissolved evaporites, or unclogged fractures. High permeability zones can also  
 132 affect local groundwater flow. All geological formations of the basin have been monitored separately  
 133 since September 2018, where measurements regarding water head H and temperature T in boreholes  
 134 have been taken (SAFEGE, 2019). On the basis of the monitoring, a characterization of the hydraulics

135 for each of the main geological formations near the Oeillal spring was conducted (Sivelle and Jourde,  
 136 2020).

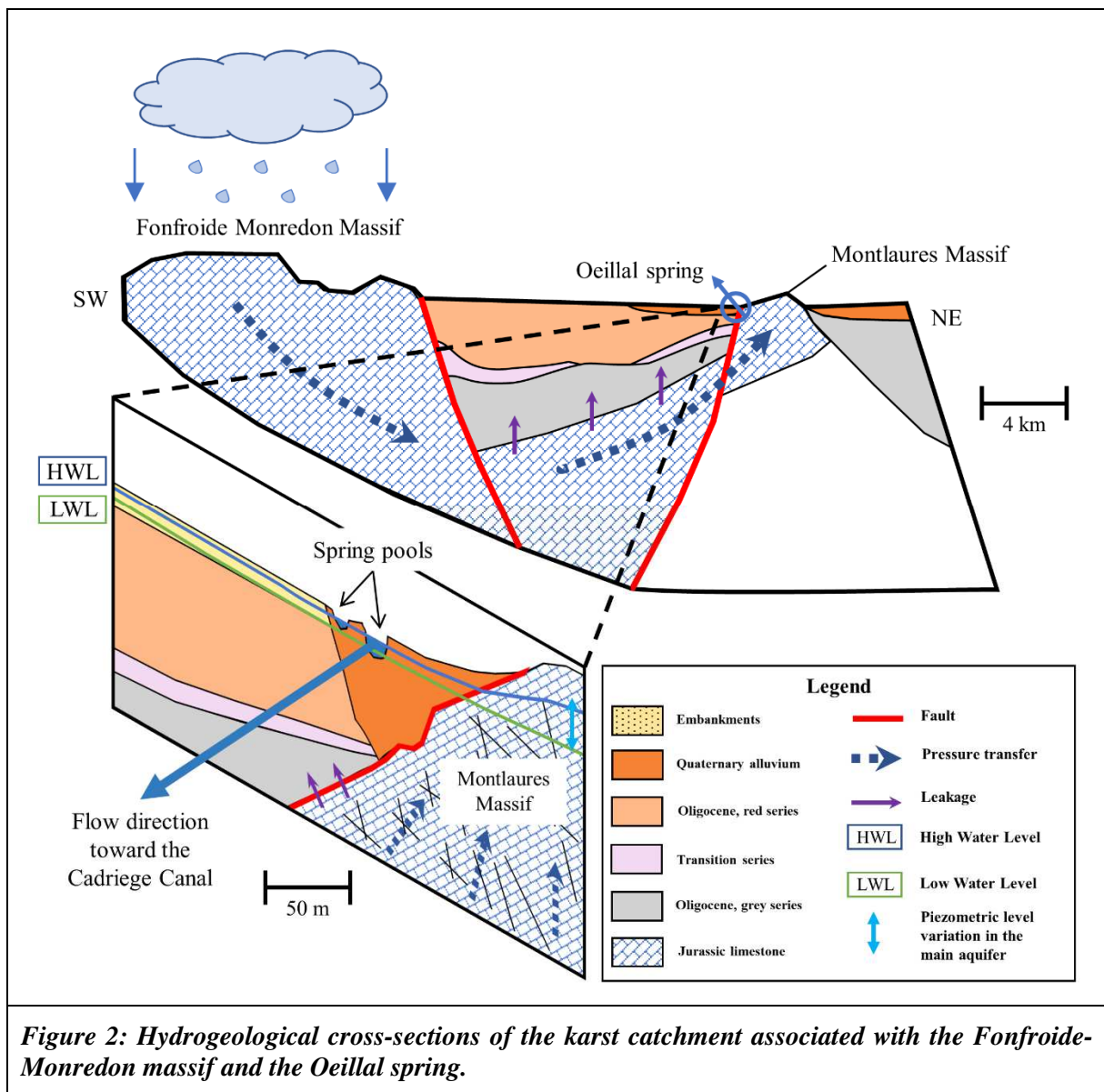


**Figure 2: Hydrogeological cross-sections of the karst catchment associated with the Fonfroide-Monredon massif and the Oeillal spring.**

137 The Oeillal spring discharge has been measured once an hour since July 2018. Besides the high-  
 138 resolution time series, long-term temporal data of the total discharge at Oeillal spring exists on a monthly  
 139 basis (measurements were performed once a month, however on varying dates). The monthly  
 140 measurements cover a period of 30 years which is available for the calibration of the hydrological model.  
 141 Although the resolution of the time series of the discharge is rather low, first hydrodynamic modeling  
 142 has been performed (Sivelle and Jourde, 2020) using a lumped parameters model implemented in the  
 143 KarstMod modeling platform (Jourde et al., 2015; Mazzilli et al., 2019). On the basis of the time series

144 analysis and the modeling, the water volume stored in the aquifer and the annual volume of transit were  
145 estimated to be appr. 7.5 Mm<sup>3</sup> and 4.2 Mm<sup>3</sup>, respectively. The karst system shows a slow recession  
146 dynamic as suggested by a regulating power of around 1.8 years and a characteristic time of the transfer  
147 function of around 200 days (Sivelle and Jourde, 2020).

148 Based on the geological map and surface river network analysis, the recharge area covers an area of  
149 appr. 42.3 km<sup>2</sup>, while lumped parameters model calibration estimated the recharge area to be 44.0 to  
150 49.4 km<sup>2</sup> (Sivelle and Jourde, 2020). The difference in the estimations could be due to the model  
151 accounting for an additional zone that potentially contributes to the recharge area through surface runoff  
152 (Figure 1). However, the impact of the additional water inflow cannot be properly quantified thus far.

## 153 **2.2 Climate**

154 The area is characterized by a Mediterranean climate with a mean annual cumulative rainfall of about  
155 550 mm (the annual cumulative rainfall varies between 300 and 1,200 mm). On average appr. 55 days  
156 of rain can be observed per year, whereby major rainfall events mainly occur in autumn with maximum  
157 rainfall intensity greater than 100 mm/day. Indeed, the area is subject to extreme precipitation events  
158 so-called “Cévenol episodes” named after the Cévennes region which lies between the Massif Central  
159 mountainous region and the Mediterranean plains (Delrieu et al., 2009). In case of snow event in the  
160 region, snowmelt can be at the origin of direct infiltration over the study area. However, such influence  
161 occurs very few due to the regional climate and the low elevation of the karst spring’s catchment (lower  
162 than 250 m a.s.l.). There are five meteorological stations operated by Météo-France (French  
163 meteorological institute) located in the study area: Argeliers, Narbonne, Narbonne-Egassairol, Fleury,  
164 and Gruissan-INRA. Based on the data from these stations, a precipitation time series with a daily  
165 resolution was constructed for the 1960-2020 period as well as a continuous temperature time series for  
166 the 1980-2020 period. With the help of the reconstruction of the time series (Sivelle and Jourde, 2020),  
167 the increasing trend around +0.4°C/decade in the mean annual temperature in Southern France since the  
168 late 1970s was accounted for (Lelièvre et al., 2010; Lespinas et al., 2010; Moisselin et al., 2002). Also,  
169 the potential evapotranspiration can be estimated through the formula proposed by Oudin et al. (2005)  
170 as suggested in a previous study over the Oeillal spring karst catchment (Sivelle and Jourde, 2020).

### 171 **2.3 Land-use and groundwater abstraction**

172 The karst aquifer is subject to anthropogenic impact through both the surface land-use and groundwater  
173 abstraction. Based on the Corine Land Cover (CLC) 2012 maps (European Environment Agency &  
174 Copernicus Land Service., n.d.), the total landcover of the recharge area shows four types of land-use:  
175 (1) quarries covering 2% of the total area, (2) urban areas, counting 1477 inhabitants (according to the  
176 census in 2017 from the French Institute of Statistics and Economic Studies INSEE), covering 4.5% of  
177 the total area, (3) vineyards and agricultural plots covering 30.8% of the total area, and (4) forests and  
178 natural plots covering 62.7% of the total area (Figure 3). Water from the karst aquifer is extracted  
179 through two pumping stations in order to provide the Narbonne agglomeration with drinking water. The  
180 pumping stations Les Mailloles (Moussan) and Croix Blanche (Montredon) have an annual groundwater  
181 abstraction volume of 0.25 Mm<sup>3</sup>/year and 0.4 Mm<sup>3</sup>/year respectively (Figure 4) wherefore drinking  
182 water constitutes the main use of the karst aquifer. Although groundwater is also used in agriculture and  
183 industry in the region, for these uses, water is mostly withdrawn from surface water. The groundwater  
184 abstraction for the quarries is with 25,000 m<sup>3</sup>/year negligible compared to the total volume abstracted  
185 for the drinking water supply. Considering the poor temporal resolution of the spring discharge time  
186 series before 2018, the effects of the water abstraction on the Oeillal spring cannot be properly assessed,  
187 especially after the Mailloles pumping station was commissioned in 2007. The total annual volume of  
188 groundwater abstraction in the karst aquifer represents around 15 to 20% of the annual volume of transit.  
189 As a comparison, in the Lez system (South of France), the groundwater withdrawal represents up to  
190 50% of the volume of transit and the system is subject to strong social and economic issues (Jourde et  
191 al., 2014). Furthermore, over-pumping may cause the spring source to dry up, as can be observed in  
192 other karst systems in the Mediterranean area (Hartmann et al., 2014; Kazakis et al., 2018; Stevanović,  
193 2019).

194 In 2030, the usage of fresh water from Croix Blanche is estimated to reach an annual volume of 0.57  
195 Mm<sup>3</sup> (ENTECH, 2016) which is more than double the mean annual volume extracted during the period  
196 of 1997-2018. Moreover, a new pumping station will be commissioned in the immediate future which  
197 will extract a maximum of 0.2 Mm<sup>3</sup>/year, which equals 30% of the current groundwater withdrawal in

198 the main aquifer (0.65 Mm<sup>3</sup>/year). Thus, predicting the development of groundwater resources in the  
 199 region requires the consideration of both, the increase in water abstraction due to human activities  
 200 (growing urban area and growing needs in freshwater), and the effects of climate change (Vörösmarty  
 201 et al., 2000).

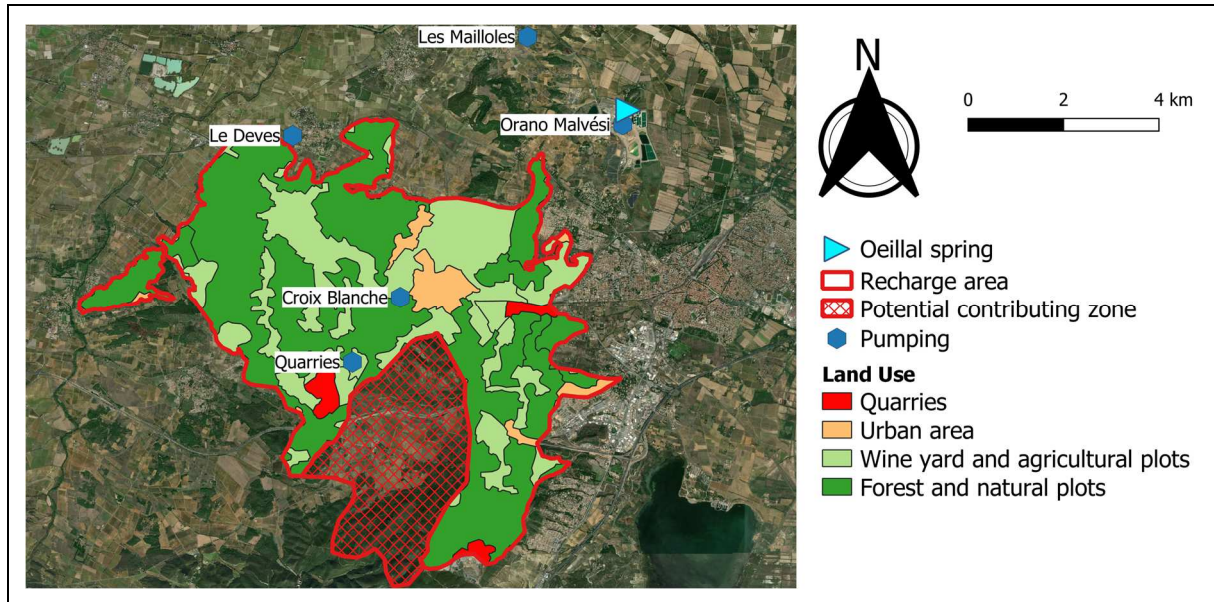


**Figure 3: Land use and pumping stations in the recharge area of the karst system associated with the Oeillal spring. The land use is determined based on the CORINE Land Cover - CLC12 (<https://www.data.gouv.fr/fr/datasets/corine-land-cover-occupation-des-sols-en-france/>)**

202

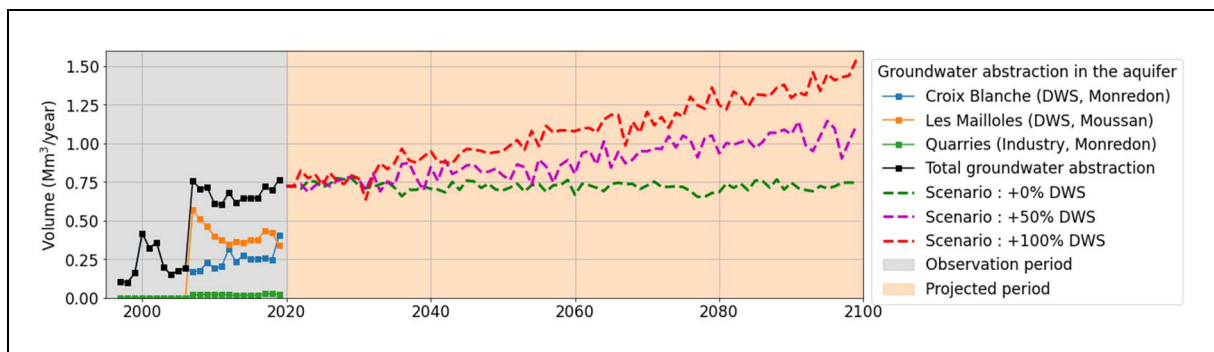


**Figure 4: Volume of groundwater abstraction in the Jurassic calcareous formation around the Malvesi area, DWS = Drinking Water Supply. The annual groundwater abstraction volumes for the observation period are provided by the Rhône-Mediterranean water agency (<https://rhone-mediterranee.eaufrance.fr/telechargement-des-donnees-de-prelevements>) and projections are made according 3 scenarios depending on the future needs in fresh water supply.**

203 **3 Material and methods**

204 **3.1 Hydrological models**

205 **3.1.1 Hydrological model structures**

206 Three lumped parameters models are implemented to account for conceptual uncertainties in the choice  
 207 of the hydrological model (HM) structure (Figure 5). The ensemble of models comprises different  
 208 conceptualizations of the karst hydrological processes of interest for which different degrees of  
 209 heterogeneity is accounted for. I.e. the KarstMod model assumes homogeneous recharge processes at  
 210 the catchment scale in the vadose zone (Mazzilli et al., 2019), while the LuKARS model considers the  
 211 impact of land-use and soil properties on recharge processes (Bittner et al., 2018). The latter thereby  
 212 simulates hydrological processes as a function of land-use and soil type which together form so-called  
 213 “hydrotopes”. The model, hence, accounts for a higher level of heterogeneity in the vadose zone.

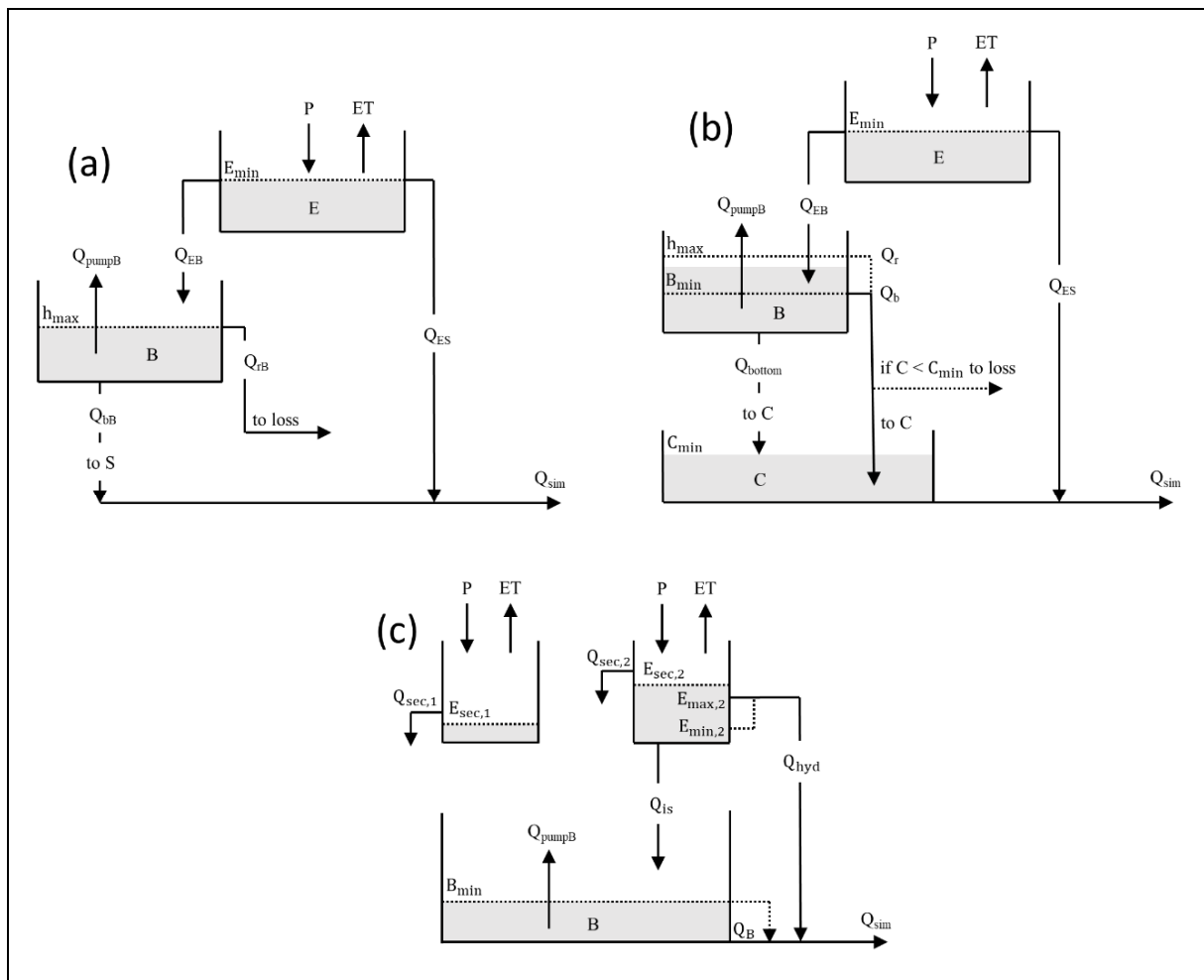


**Figure 5: Hydrological model ensemble: (a) model implemented in the KarstMod modeling platform (denoted HM\_1); (b) modified KarstMod model, including a ceiling effect in the lower compartment (denoted HM\_2); (c) model implemented based on the LuKARS model considering an impervious zone and an infiltration zone (denoted HM\_3).**

214 At first, a hydrological model (Figure 5 a, denoted HM\_1) was implemented based on the KarstMod  
215 modeling platform (Jourde et al., 2015; Mazzilli et al., 2019). A detailed description of KarstMod and  
216 its underlying equations is provided in Appendix A. The model consists of two interconnected  
217 compartments: an upper compartment E and a lower compartment B characterized by a transfer function  
218 with an infinite characteristic time (Guinot et al., 2015). The model structure HM\_1 was initially  
219 proposed by Sivelles and Jourde (2020). The model is sufficiently capable of estimating the groundwater  
220 resources variability, however fails to reproduce the quick dry-up of the Oeillal's spring observed during  
221 low flow periods due to the neglect of the threshold effect in the recession coefficient which depends  
222 on the piezometric level in the karst aquifer (change in the recession coefficient for a piezometric level  
223 = 6.5 m a.s.l.).

224 Although the threshold effect was determined through piezometric and spring discharge time series,  
225 neither a conceptualization nor implementation in a conceptual model have been proposed, yet. To  
226 account for the uncertainty in the conceptualization of both the model structure and the threshold effect,  
227 the study followed different conceptualizations approaches. Considering the potential effect of the major  
228 fault due to the bordering Montlaures massif (Figure 2), one approach applied a flow routine from the  
229 baseflow compartment as a function of the water level for which a disconnection of a part of the drainage  
230 system from the spring was observed. This could explain the spring discharge deficit during low flow  
231 conditions, when the piezometric level in the main aquifer is lower than 6.5 m a.s.l. which principally  
232 occurs during summer season. Another conceptualization assumed losses to occur downstream of the  
233 spring pool. In this case, the recession dynamics in the lower compartment solely depend on the water  
234 level in this compartment. The present study thus better accounts for the complexity in hydrological  
235 models (Figure 5) than the former study by Sivelles and Jourde (2020) and is thereby capable of  
236 incorporating the threshold effect of the Oeillal spring discharge.

237 The first conceptualization mentioned hereabove was implemented in the KarstMod model. A threshold  
238 effect was considered in compartment B which is affected by the water level in the lower compartment  
239 C (Figure 5 b, denoted HM\_2). When the water level in C is sufficiently high, there is a hydraulic  
240 continuity of the baseflow from compartment B to compartment C (fluxes  $Q_b$  and  $Q_r$ ) and subsequently

241 to the spring. On the opposite, when the water level decreases, the continuity is no longer sufficient,  
242 wherefore for both fluxes,  $Q_b$  and  $Q_r$ , loss occurs. The reason for the observed threshold effect and its  
243 associated hydrodynamic behavior thereby probably lies in the water level dependent disconnection of  
244 some parts of the drainage system (Figure 2) as observed for other karst systems such as the Lez aquifer  
245 (Clauzon et al., 2020; Dausse et al., 2019).

246 The third hydrological model (Figure 5 c, denoted HM\_3) is based on the LuKARS model (Bittner et  
247 al., 2018, 2020b) in which hydrotopes (characterized by land use and soil type) conceptually represent  
248 the vadose zone compartment (higher level with the continuum soil-epikarst-infiltration zone). The  
249 vadose zone is connected to the saturated zone compartment (lower level) characterized by a linear  
250 baseflow compartment (a detailed description of LuKARS and its equations is provided in Appendix  
251 B). Although the recharge area is mainly composed of carbonate rock outcrops with poor soil  
252 development, four different land-use types exist in the recharge area (Figure 3). Quarries and urban areas  
253 are assumed to be impervious covers, hence surface water run-off for these areas does not contribute to  
254 the aquifer recharge, as suggested by Bittner et al. (2018, 2020b). In the model, quarries and urban areas  
255 belong to the same hydrotipe characterized by a null flux towards the baseflow compartment B.  
256 Infiltration, on the contrary occurs in vineyards, agricultural and natural plots as well as forest areas  
257 which contribute to the recharge of the baseflow compartment B.

258 The second conceptualization mentioned hereabove considers the threshold effect to be directly related  
259 to the structure of the model and a change in the recession coefficient at the spring to depend on the  
260 water level. In this case (Figure 5 c), the lower part of the linear baseflow compartment B is characterized  
261 by a higher recession coefficient which allows the reproduction of the quick-drying-up observed during  
262 low flow period at the Oeillal spring. The spring discharge, hence, shows a slow recession dynamic  
263 when the water level in compartment B is greater than  $B_{min}$ . When the water level in compartment B  
264 decreases and becomes lower than  $B_{min}$ , the spring discharge shows a faster recession dynamic.  
265 Between the low and high flow conditions, measurements showed that the recession coefficient  
266 increases by appr. one order of magnitude.

### 267 **3.1.2 Calibration and validation**

268 The three hydrological models (HM) were implemented in the R environment (R Core Team, 2013),  
269 while the parameter estimation was performed using a Particle Swarm Optimization (PSO) procedure  
270 implemented with the “pso” package (Bendtsen, 2012). The data set for the calibration and validation  
271 of the hydrological models is composed of continuous daily rainfall and temperature time series data for  
272 the 1980-2020 period, monthly discharge measurements for the 1987-2017 period and daily discharge  
273 measurements for the 2018-2020 period. The objective function for the hydrological models' calibration  
274 represents a weighted sum of the widely used Kling-Gupta efficiency KGE (Gupta et al., 2009) as well  
275 as the modified balance error BE (Perrin et al., 2001) :

$$W_{obj} = w \times KGE(Q) + (1 - w) \times BE(Q) \quad \text{Eq. 1}$$

276 where  $W_{obj}$  is the objective function to be maximized through calibration and  $w$  refers to the user-  
277 defined weight ( $0 \leq w \leq 1$ ). In our study, the hydrological models are calibrated using  $w = 0.75$  (Sivelle  
278 and Jourde, 2020). Considering the discrepancy in temporal resolution between monthly discharge data  
279 from 1987-2017 and daily discharge data from 2018-2020, the hydrological models were calibrated for  
280 the period of 2018-2020. The period of 1987-2017 was used for validation purposes.

### 281 **3.2 Regional climate change projections**

282 To account for future climate change scenarios, a sub-set of representative simulations was selected  
283 from the high-resolution (12.5 km<sup>2</sup>) regional climate model (RCM) from the EURO-CORDEX  
284 experiment (Jacob et al., 2020, 2014). RCMs downscale the General Circulation Models (GCMs)  
285 simulations of the Coupled Model Intercomparison Project Phase 5 (CMIP5) (Taylor et al., 2012). In  
286 this study, each GCM is two different RCMs to assess uncertainties in terms of GCM/RCM combinations  
287 (Table 1). The six GCMs used in this study were found to be adequate for Europe (McSweeney et al.,  
288 2015; Vautard et al., 2020). More information about the description of the RCMs and GCMs in the Euro-  
289 CORDEX experiment can be found in Jacob et al., (2014). Furthermore, the two Representative  
290 Concentration Pathway (RCP) most commonly used in climate change impact studies in our region of

291 interest were retained: the “intermediate” RCP 4.5 (stabilization of radiative forcing after the 21<sup>st</sup> century  
 292 at 4.5 W/m<sup>2</sup>) and the “adverse” RCP 8.5 (rising radiative forcing crossing 8.5 W/m<sup>2</sup> at the end of 21<sup>st</sup>  
 293 century).

Institute	Regional Climate Models (RCM)	General Circulation Models (GCM)					
		CNRM-CM5	EC-EARTH	IPSL-CM5	HADGEM2	MPI-ESM	NorESM1
SMHI	RCA4	X	X	X	X	X	X
CLM	CCLM4.8.17				X		
CNRM	ALADIN5.3	X					
DMI	HIRHAM5.1						X
KNMI	RACMO2.2		X				
IPSL	WRF3.3.1			X			
MPI	REMO2009					X	

*Table 1 Matrix of the RCM/GCM simulations*

294 The simulated RCM data (for each RCP) was adjusted to avoid biases for the period of 1960–2005 and  
 295 1990-2005 for rainfall and temperature, respectively. The bias correction was performed using the  
 296 quantile mapping methodology (Déqué, 2007; Grillakis et al., 2013). According to this method, the  
 297 probability density function of the simulated data is corrected based on the observed time series to  
 298 eliminate the errors due to downscaling from GCM to RCM (Figure 6). The procedure was performed  
 299 for all climate models for the RCP 4.5 and RCP 8.5 scenarios. The corrected simulated temperature time  
 300 series, hence, estimates the potential evapotranspiration according to the Oudin’s formula (Oudin et al.,  
 301 2005).

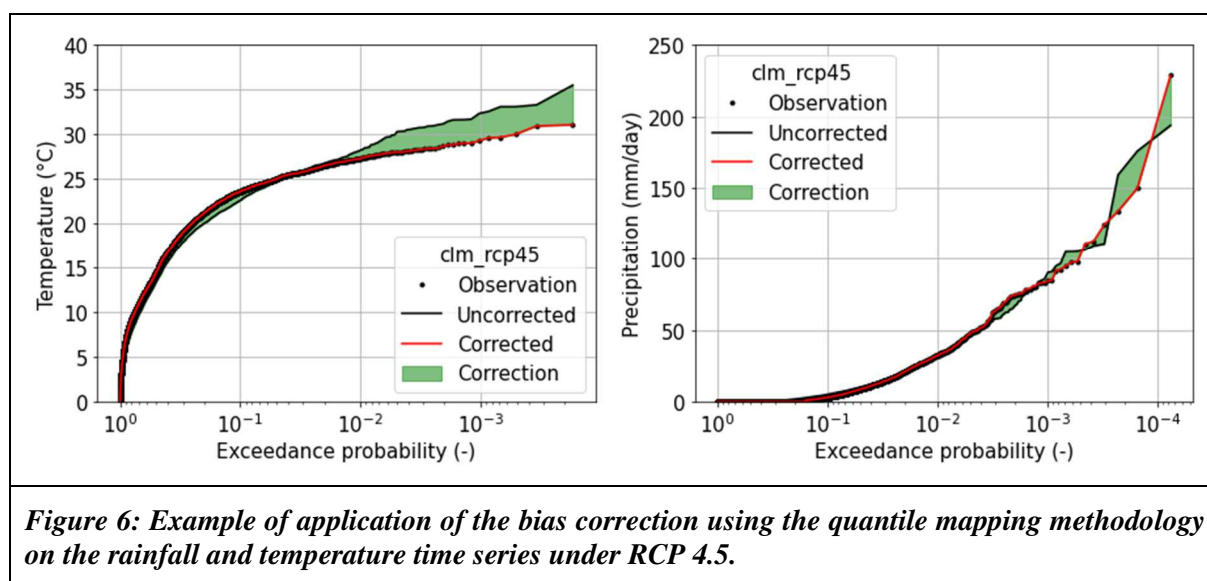


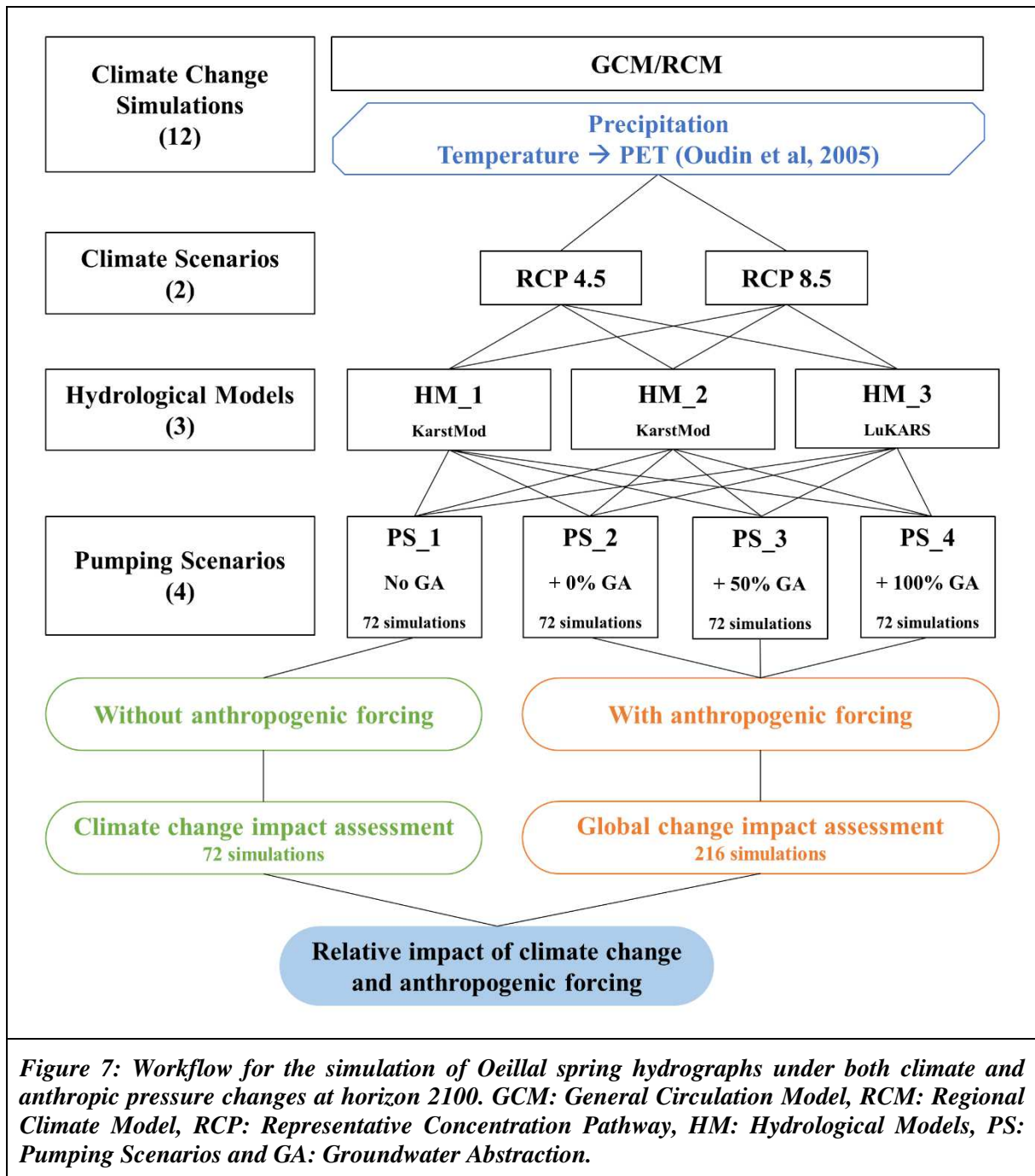
*Figure 6: Example of application of the bias correction using the quantile mapping methodology on the rainfall and temperature time series under RCP 4.5.*

302 In this study, the simulated rainfall and temperature time series are derived from the EURO-CORDEX  
303 simulation grid. Although the Oeillal spring's recharge area is covered by a single unit grid cell in the  
304 EURO-CORDEX simulations, several observations were found suitable in order to assess the potential  
305 future climate variables (i.e. rainfall and temperature) for the catchment of the Oeillal spring (Figure 1).

### 306 **3.3 Coupling climate changes and anthropogenic pressures scenarios**

307 The proposed workflow (Figure 7) consists of testing several scenarios considering an ensemble of 12  
308 climate model simulations (Table 1), two climate scenarios (RCP 4.5 and RCP 8.5), three hydrological  
309 models (HM\_1 to HM\_3) and four pumping scenarios (PS\_1 to PS\_4). The different pumping scenarios  
310 account for the range of future anthropogenic pressures. PS\_1 considers no groundwater abstraction in  
311 the karst aquifer and allows to assess the Oeillal spring discharge without anthropogenic forcing. PS\_2  
312 assumes that the mean annual groundwater abstraction remains the same as in present-day. PS\_3 and  
313 PS\_4, on the contrary, assume an increasing water abstraction (+50 % and +100%, respectively) until  
314 2100 based on predictions in terms of future needs of freshwater supply.

315 The application of the proposed workflow allows to simulate 288 hydrographs, where 72 simulations  
316 consider the effects of climate change without anthropogenic forcing and 216 simulations consider the  
317 combined effects of climate changes and anthropogenic forcing under different scenarios. The  
318 application of three different model conceptualizations thereby accounts for output uncertainties related  
319 to climate change projections and conceptual model uncertainties. Finally, the comparison of the  
320 simulated spring discharge considering anthropogenic forcing (PS\_1) with the simulated spring  
321 discharge considering different scenarios in the future need in drinking water supply (PS\_2 to PS\_4)  
322 allows to assess the relative impact of the climate change and the anthropogenic forcing. Indeed, the  
323 simulated hydrographs considering PS\_1 allow estimating the impact of climate change on the spring  
324 discharge without any anthropogenic forcing and so can be considered as a “naturalized” spring  
325 discharge. Then, comparison of such “naturalized” discharge with the simulated spring hydrograph  
326 under different pumping scenarios (PS\_2 to PS\_4) allows assessing the potential consequences for  
327 groundwater abstraction on the spring discharge as well as the relative impacts of the climate change  
328 and the anthropogenic forcing.



329 **4 Results and discussion**

330 **4.1 Hydrological models' calibration and validation**

331 The calibrated parameter sets for HM\_1 and HM\_2 (based on the KarstMod modeling platform) are  
 332 reported in Table 2, whereas the parameters for HM\_3 (based on the LuKARS model) are reported in  
 333 Table 3. Table 4 summarizes the performance criteria for the calibration and validation periods, i.e. with  
 334 continuous spring discharge data (2018-2020) and sparse spring discharge data (1987-2017),

335 respectively. All three hydrological models perform satisfactorily for the calibration period, whereby  
336 HM\_3 outperforms the other two models. The performance for the validation period, on the contrary, is  
337 rather low most likely due to the use of sparse spring discharge time series that is hardly capable of  
338 representing the hydrodynamics of a karst system as has been suggested in earlier studies (Sivelle and  
339 Jourde, 2020).

340 The simulated hydrograph of HM\_2 closely resembles the simulated hydrograph of HM\_1 until 2016.  
341 Over the 1987-2017 period, despite the low resolution of the time series data, an overall decreasing trend  
342 of the mean spring discharge is visible. After 2016, the inclusion of the threshold effect of HM\_2  
343 becomes apparent which more realistically reproduces the quick dry-up observed during the calibration  
344 period (Figure 8). Although the analysis of the simulated hydrograph highlights the significant impact  
345 of the threshold effect on hydrological models, the performance assessment for HM\_1 and HM\_2 is  
346 rather similar. For the HM\_3, the effects of the threshold are already apparent in the early 2000s, while  
347 also better capturing the dynamics in certain periods (such as 1992-1996) and limiting spring discharge  
348 overestimations (as can be observed for 1994, 1996 and 2004). The comparison of the simulated spring  
349 hydrographs shows the importance of applying several hydrological models in order to account for  
350 conceptualization and parametric uncertainties. Note, however, that these uncertainties were not  
351 evaluated in this study.

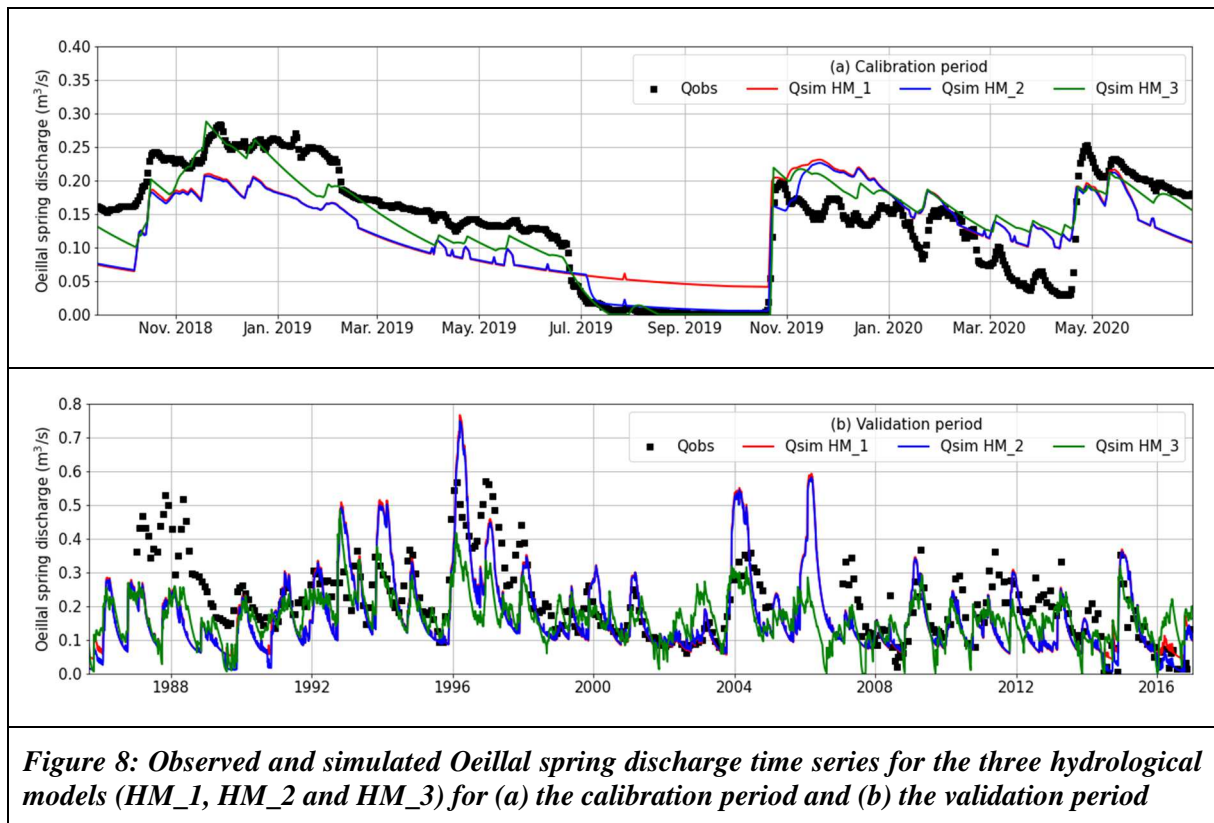


**Figure 8: Observed and simulated Oeillal spring discharge time series for the three hydrological models (HM\_1, HM\_2 and HM\_3) for (a) the calibration period and (b) the validation period**

Compartment	Parameter	Description	Unit	Model	
				KM_1	KM_2
-	Ra	Recharge area	km <sup>2</sup>	42.3	42.3
E	E0	Initial water level in E	Mm	32.3	32.3
	kES	Recession coefficient from E to S	mm.day <sup>-1</sup>	1.64×10 <sup>-2</sup>	1.64×10 <sup>-2</sup>
	kEB	Recession coefficient from E to B	mm.day <sup>-1</sup>	8.76×10 <sup>-2</sup>	8.76×10 <sup>-2</sup>
	Emin	Minimum water level in E	Mm	10.3	10.3
B	B0	Initial water level in B	Mm	350	350
	alpha	Exponent for the infinite time scale transfer function	-	0.79	0.75
	hmin	Lower threshold	Mm	0	0
	hmax	Upper threshold	Mm	∞	∞
	tau0	Time scale	Day	150	150
	Bmin	Threshold in sub-compartment in the compartment B	Mm	-	35
C	C0	Initial water level in C	Mm	-	0
	kCS	Recession coefficient from C to S	mm.day <sup>-1</sup>	-	4.18×10 <sup>-1</sup>
	Cmin	Threshold for the orientation of overflow fluxes from the compartment B	Mm	-	0.29

**Table 2: Calibration values of the model parameters for KarstMod models.**

353

Compartment	Parameter	Description	Unit	Model
				HM_3
-	Ra	Recharge area	km <sup>2</sup>	42.3
E1 Impervious zone	kES	Discharge parameter for QES	m mm <sup>-1</sup> .d <sup>-1</sup>	0
	Emin	Minimum storage capacity	Mm	0
	Emax	Maximum storage capacity	Mm	1
	alpha	Hydrotope-specific quickflow exponent	-	0
	kEB	Discharge parameter for QEB	m mm <sup>-1</sup> .d <sup>-1</sup>	0
	kloss	Discharge parameter for Qloss	m mm <sup>-1</sup> .d <sup>-1</sup>	3.9
	Esec	Activation level for Qloss	Mm	0
E2 Infiltration zone	kES	Discharge parameter for QES	m mm <sup>-1</sup> .d <sup>-1</sup>	43.4
	Emin	Minimum storage capacity	Mm	5.1
	Emax	Maximum storage capacity	Mm	12.3
	alpha	Hydrotope-specific quickflow exponent	-	1
	kEB	Discharge parameter for QEB	m mm <sup>-1</sup> .d <sup>-1</sup>	0.21
	kloss	Discharge parameter for Qloss	m mm <sup>-1</sup> .d <sup>-1</sup>	15.0
	Esec	Activation level for Qloss	Mm	12.89
B	kBS <sub>base</sub>	Discharge parameter for QBS baseflow	m mm <sup>-1</sup> .d <sup>-1</sup>	5.29×10 <sup>-2</sup>
	kBS <sub>over</sub>	Discharge parameter for QBS overflow	m mm <sup>-1</sup> .d <sup>-1</sup>	9.78×10 <sup>-3</sup>
	Bmin	Activation level for QBS overflow	Mm	3.29

**Table 3: Calibration values of the model parameters for LuKARS model.**

Model	1987-2020					2018-2020				
	sparse discharge time series					continuous discharge time series				
	NSE	KGE	KGENP	BE	VE	NSE	KGE	KGENP	BE	VE
HM_01	0.07	0.55	0.59	0.79	0.60	0.50	0.59	0.69	0.90	0.62
HM_02	0.07	0.56	0.59	0.77	0.61	0.55	0.67	0.68	0.85	0.66
HM_03	0.14	0.34	0.49	0.77	0.62	0.78	0.85	0.84	0.98	0.79

*Table 4: Hydrological models' performances criterion between observed and simulated spring discharge (NSE: Nash Sutcliff Efficiency, KGE: Kling Gupta Efficiency, KGENP: Kling Gupta Efficiency Non-Parametric, BE: Balance Error and VE: Volume Error)*

## 354 4.2 Impacts of climate change on rainfall and potential evapotranspiration

355 To assess the impact of climate change, the time series data was divided into three non-overlapping  
356 periods of 38 years. The 1982-2020 period is based on observed data and can therefore function as a  
357 reference period. The 2021-2059 and 2060-2098 periods correspond to the near future and more distant  
358 future. During the 1982-2020 period, the annual rainfall pattern shows seasonal variations with low  
359 amounts of precipitations (< 30 mm/month) during the summer months and higher precipitations in  
360 autumn, when monthly precipitation may exceed 90 mm/month (Figure 9). Nonetheless, the monthly  
361 precipitation amount does not show the impact of significant single precipitation events that frequently  
362 occur in autumn. Within the seven episodes, cumulative precipitation amount may reach up to 290  
363 mm/day. The comparison of the rainfall projections of the 2021-2059 and 2060-2098 periods with the  
364 1982-2020 period does not allow reliable conclusions in terms of the development of monthly  
365 precipitation patterns. The projection of the potential evapotranspiration, on the contrary, shows a clear  
366 increasing trend in both periods with for all months of the year (Figure 9). The increase in potential  
367 evapotranspiration is the greatest for the RCP 8.5 for the 2060-2098 period. The maximum values (>  
368 200 mm/month) is reached during July/August when the rainfall rate is minimal (< 30 mm/month). This  
369 may lead to an increase in the water deficit, although it must be noted that actual evapotranspiration  
370 rates may differ significantly from the potential evapotranspiration due to the limited water availability  
371 in the soil and epikarst, as well as the adaptation of vegetation to changing climatic conditions (Bussotti  
372 et al., 2014; Klausmeyer and Shaw, 2009; Llorens and Domingo, 2007).

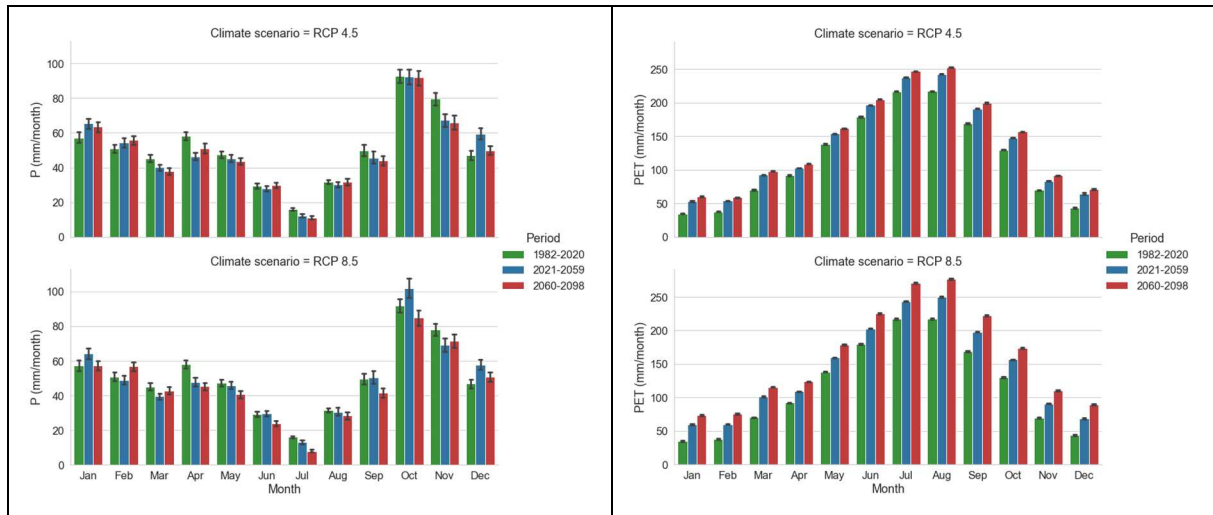


**Figure 9: Observed and climate projection mean monthly precipitation amount (left) and evapotranspiration (right) for the control period (1989-2019), the near future (2020-2050) and remote future (2060-2090) periods.**

### 373 4.3 Impacts of climate change on the spring discharge

374 The probability density function (PDF) of the spring discharge without anthropogenic forcing (i.e. there  
 375 is no groundwater abstraction) is computed for the reference period (1982-2020), the near future (2021-  
 376 2059) and the more distant future (2060-2098) (Figure 10). All PDFs show a progressive shift of the  
 377 distribution towards low discharge values regardless of the severity of the climate change scenario.  
 378 Moreover, the probability of low flow (spring discharge  $< 0.1 \text{ m}^3/\text{s}$ ) increases significantly for the RCP  
 379 8.5 scenario. One should note that the threshold with spring discharge equal to  $0.1 \text{ m}^3/\text{s}$  corresponds to  
 380 the order of magnitude of the spring discharge for which a quick drying-up of the Oeillal spring is  
 381 observed (Sivelle and Jourde, 2020). Hence, for the RCP 8.5 scenario, there is a significant increase in  
 382 the occurrence of the Oeillal spring drying up.

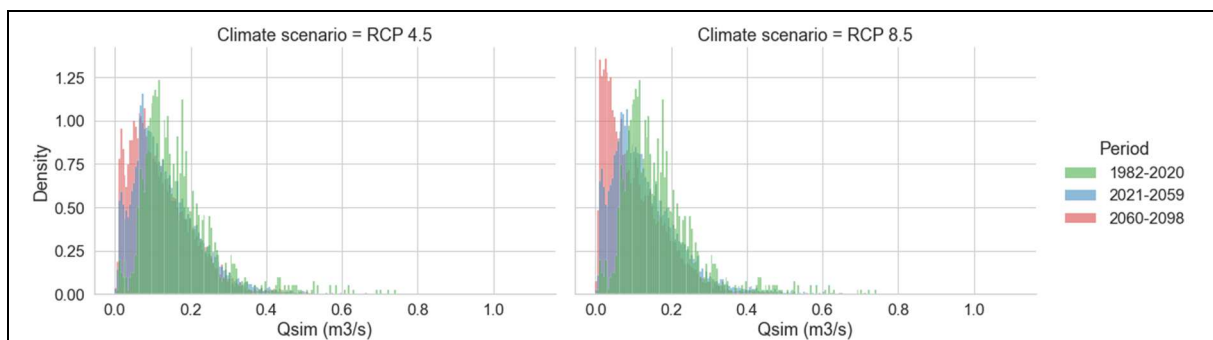
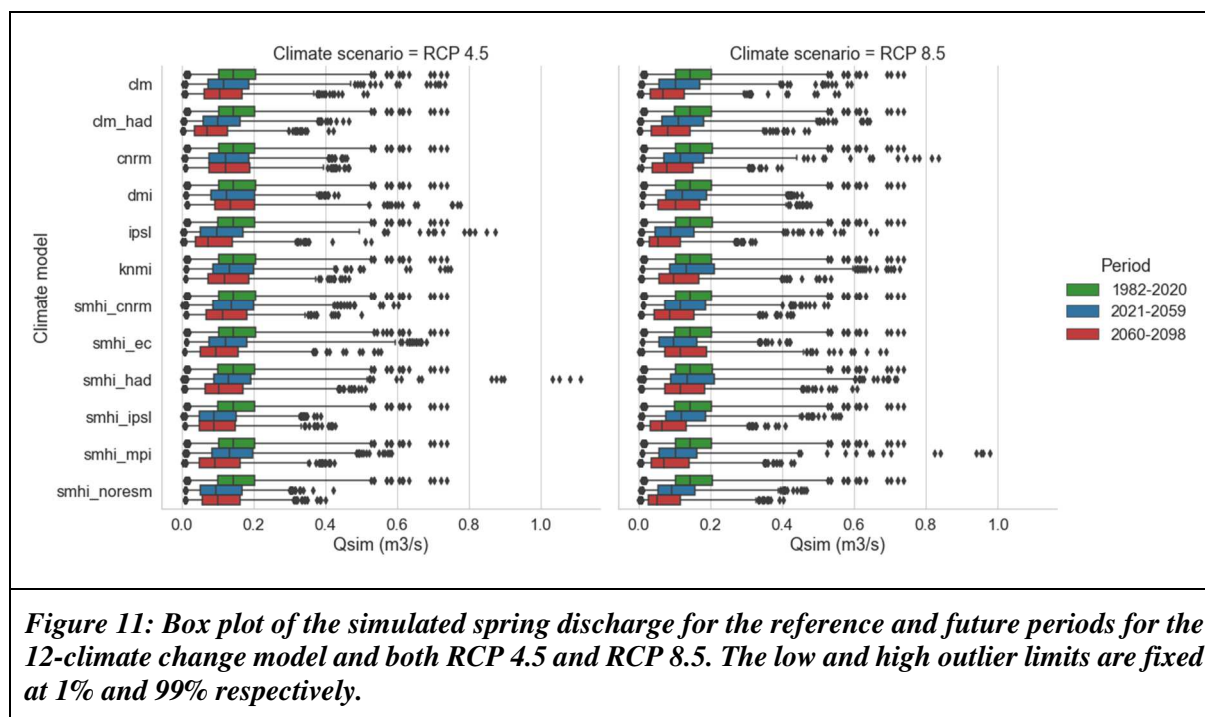


**Figure 10: Probability density function of simulated spring discharge under hypotheses on both climate change scenarios (RCP 4.5 and RCP 8.5) and no groundwater withdrawal (PS\_1).**

383 Despite the general decrease that is predicted for the Oeillal spring discharge, some high flow events  
 384 can be observed. Primarily after significant rainfall events, spring discharge exceeds 0.3 m<sup>3</sup>/s (i.e.  
 385 cevenol episodes during the October/November period). In the past, the maximum flow discharge  
 386 frequently exceeded the value of 0.3 m<sup>3</sup>/s during flood events, however in the recent years since 2015,  
 387 such high flow rates have no longer been observed (Figure 8). It is, nevertheless, difficult to draw a  
 388 reliable conclusion due to the lack of continuous daily spring discharge data before 2018. Since 2018  
 389 the flow rate of 0.3 m<sup>3</sup>/s has only been exceeded for a few hours after a significant rainfall event that  
 390 may also incorporate surface runoff and/or subsurface flow in rapid drainage structures. When  
 391 comparing the distribution for the simulated spring discharge without anthropogenic forcing, a  
 392 decreasing trend is evident for both, RCP 4.5 and RCP 8.5 scenarios (Figure 11). Despite the uncertainty  
 393 in climate changes simulation over the area the results of this study prove a clear impact of the climate  
 394 change on the Oeillal spring discharge.



#### 395 4.4 Impacts of groundwater abstraction on the spring discharge

396 The monthly mean value of the spring discharge was calculated for the reference period (1982-2020),  
 397 the near future (2021-2059) and the more distant future (2060-2098) for different assumptions in terms  
 398 of future needs for freshwater (Figure 12). Changes in the spring discharge amplitude due to an increased

399 groundwater extraction are by far less than the changes caused by climate change for both the 2021-  
400 2059 and 2060-2098 periods. Thus, the significative increase of temperature and thus of the potential  
401 evapotranspiration related to climate change, appears as the most important factor affecting the future  
402 outflow at the Oeillal spring, this decrease in discharge being aggravated by anthropogenic forcing  
403 (pumping), but to a lower extent. Indeed, there is a significant discrepancy between spring discharge  
404 without any (PS\_1) and with (PS\_2 to PS\_4) anthropogenic forcing, the latter three assume a constant  
405 groundwater abstraction, an increase of 50%, and an increase of 100% of the mean annual groundwater  
406 abstraction, respectively. Due to anthropogenic forcing, spring discharges lower than 0.1 m<sup>3</sup>/s (threshold  
407 effect leading to a quick dry-up of the Oeillal spring) occur earlier in the hydrological cycle, i.e from  
408 May to November, whereas for the most unfavorable scenario (RCP 8.5 and PS\_4), an increase in  
409 pumping additionally extends the period for potential dry-ups. For the 2060-2098 period, PS\_4  
410 groundwater abstraction levels lead to a dry period lasting at least from June to October, possibly even  
411 from April to December. The more frequent occurrence of dry periods will have a significant impact on  
412 the surface streamflow discharge in the Cadriege canal (downstream of the Oeillal spring) where surface  
413 water withdrawal is performed.

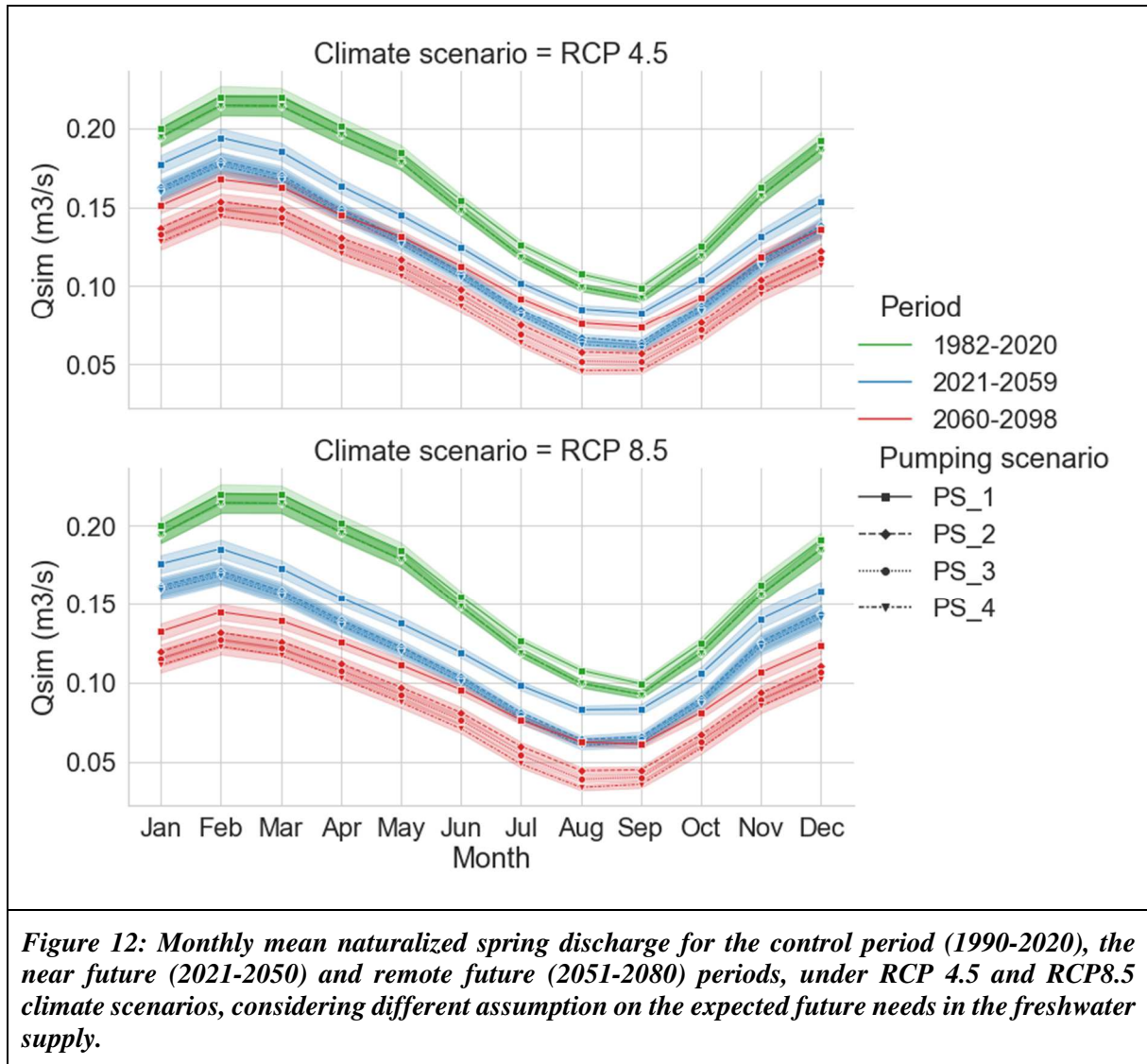


**Figure 12: Monthly mean naturalized spring discharge for the control period (1990-2020), the near future (2021-2050) and remote future (2051-2080) periods, under RCP 4.5 and RCP8.5 climate scenarios, considering different assumption on the expected future needs in the freshwater supply.**

414 Climate change and anthropogenic forcing have a significant influence on the Oeillal spring discharge  
 415 for the near (2021-2059) and more distant future (2060-2098). Although climate change has a major  
 416 effect on spring discharge (Figure 12), groundwater abstraction significantly effects the frequency of  
 417 the drying-up of the Oeillal spring (Figure 13).

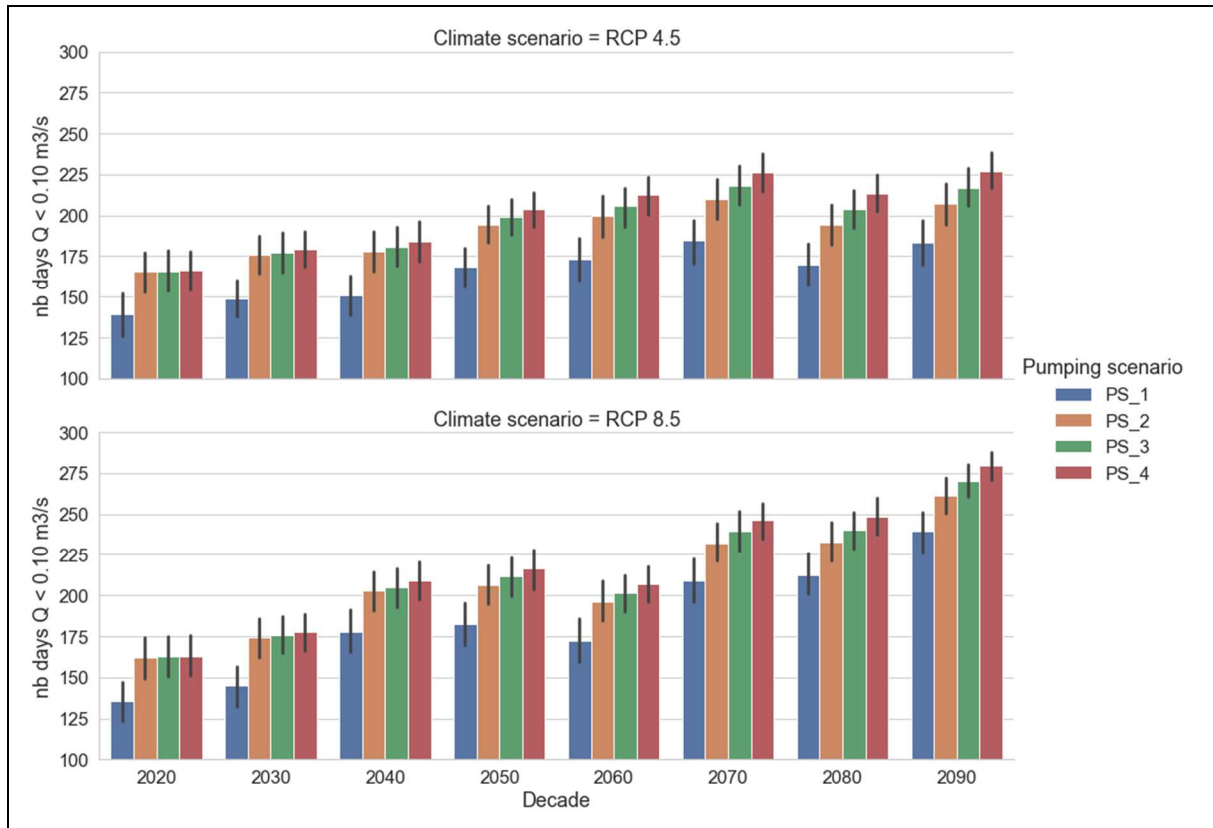
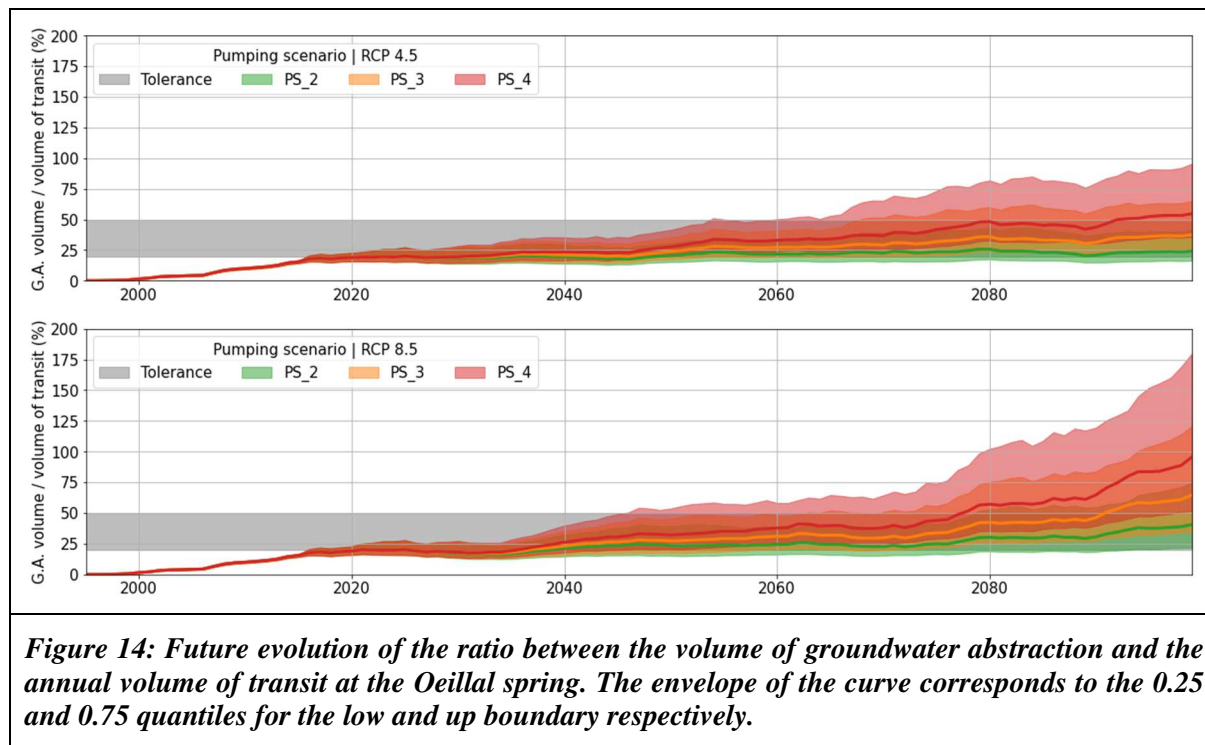


**Figure 13: Mean number of days per year with a simulated spring discharge lower than 0.1 m³/s for each decade starting from 2020 to 2090.**

#### 418 **4.5 Relative impacts of groundwater abstraction and climate changes**

419 Figure 14 shows the projection of the ratio between groundwater abstraction and the annual volume of  
 420 transit (i.e. the total volume of water passing through the Oeillal spring) according to the future needs  
 421 in freshwater (PS\_2 to PS\_4). Most of the scenarios, which account for both climate and groundwater  
 422 abstraction changes, show a constant increase in the imbalance between groundwater abstraction and  
 423 the volume of transit at the Oeillal spring. Indeed, all scenarios predict the ratios between groundwater  
 424 abstraction and volume of transit at the Oeillal spring to increase after 2020. The six global change  
 425 scenarios (all combinations of the RCPs and the pumping scenarios) cover a wide range of projections.  
 426 For both RCP 4.5 and RCP 8.5, the ratio seems to stabilize by 2060-2070. For the RCP 8.5, some models  
 427 predict that the annual groundwater abstraction may exceed the annual volume of transit at Oeillal spring  
 428 completely at horizon 2080. Nonetheless, this was only the case for the most unfavorable scenario (a  
 429 combination of RCP 8.5 and PS\_4). For the most favorable pumping scenario (PS\_2), where the  
 430 groundwater abstraction is supposed to be a present-day abstraction, the ratio between groundwater

431 abstraction and the annual volume of transit show a slight increase. This demonstrates that part of the  
 432 forecasted imbalance is directly the consequences of the climate change on the spring discharge, which  
 433 also can be aggravated by groundwater abstraction.



434 Previous results highlighted that climate change will have a massive impact on the Oeillal spring  
 435 discharge and that groundwater abstraction may act as an aggravating factor in the drying up of the  
 436 Oeillal spring. To better assess the influence of anthropogenic forcing concerning climate change, we  
 437 plotted the difference between predicted spring discharge and the reference period with and without  
 438 groundwater extraction. Figure 15 thus allows assessing the relative contributions of groundwater  
 439 extraction and climate change on the Oeillal spring discharge. The simulated spring discharge for the  
 440 future groundwater extraction scenarios PS\_2 to PS\_4 was compared to the simulated spring discharge  
 441 without anthropogenic forcing (PS\_1). The results highlight that under severe climate change (RCP 8.5),  
 442 groundwater abstraction has a significant impact regardless of the amount. An increase in groundwater  
 443 extraction as assumed in PS\_4 may in fact induce a decrease of up to 25% of the mean annual spring  
 444 discharge. This means that the groundwater extraction will be responsible for one-quarter of the spring  
 445 discharge decrease. This emphasizes once more that climate change is still the predominant factor  
 446 influencing the future evolution of the studied Mediterranean spring.

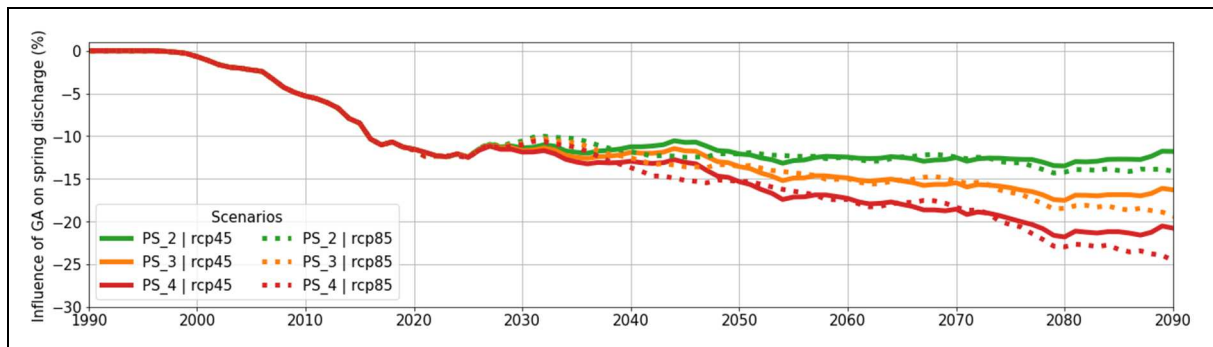


**Figure 15: Evolution of the influence of the groundwater abstraction (GA) on the Oeillal spring discharge.**

447 As groundwater extraction in the study area is mostly used for drinking water supply for the Narbonne  
 448 agglomeration, tourism is the main reason why water needs will increase during the summer season.  
 449 Although the groundwater extraction may induce up to 25 % of the annual mean spring discharge  
 450 decrease, it may account for up to 30% for the 2021-2059 period and up to 40% for the 2060-2098  
 451 period (Figure 16).

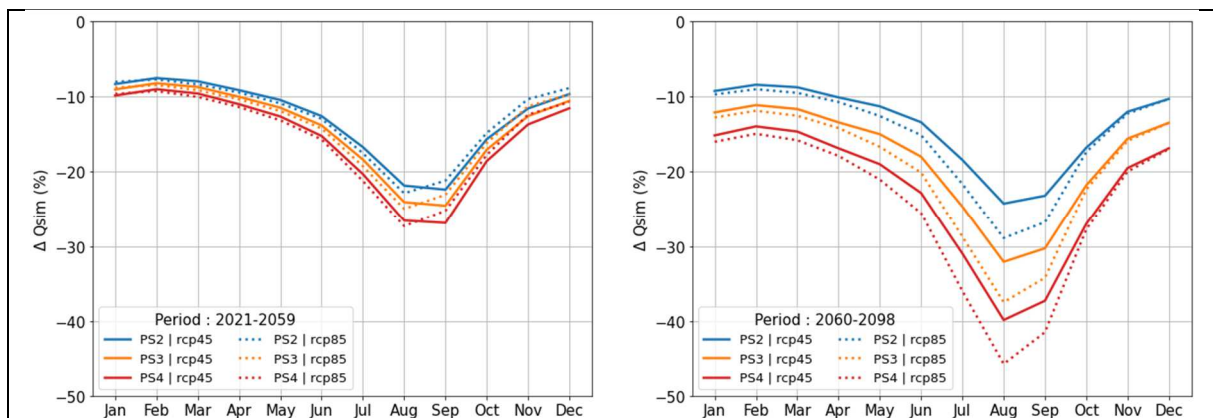


**Figure 16: Influence of the groundwater abstraction on the monthly mean spring discharge under various global changes assumption.**

#### 452 4.6 Transferability and limitations of the workflow

453 The present study regards a Mediterranean karst aquifer subject to anthropic pressure which is an  
 454 important freshwater resource for the Narbonne agglomeration (Southern France). Not only the  
 455 Narbonne region, but various large cities in the Mediterranean depend on karst aquifer groundwater  
 456 resources emphasizing the importance of assessing the future development of karst groundwater  
 457 resources in the basin. The transferability of the present study to other karst aquifers is rather limited  
 458 due to the assumptions made in the study.

459 The proposed workflow only accounts for changes in groundwater extraction, while LCLU changes  
460 were not addressed in this study. In future research, the response of karst vegetation to climate change  
461 and human activities should also be addressed (Zhao et al., 2020) as this may have a strong impact on  
462 the catchment hydrology (Cosandey et al., 2005). The use of dedicated hydrological model considering  
463 land-use changes (Bittner et al., 2018) and semi-distributed recharges (Ollivier et al., 2020) can be of  
464 interest to assess the potential effects of such changes and contribute to a better understanding of  
465 groundwater variability in karst catchments.

466 The proposed workflow included three hydrological models in order to eliminate conceptualization and  
467 parametric uncertainties, however it does not evaluate them. Since the hydrological models consist of  
468 different level of complexity (and require additional parameters), one should apply the principle of  
469 parsimony to avoid over parametrization (Perrin et al., 2001). In complex karst system, it is much easier  
470 to reproduce hydrological processes with a high dimensional parameter space (Hartmann, 2018) but a  
471 large number of calibration parameters can cause over parametrization, wherefore parameters can lose  
472 their identifiability (Hartmann et al., 2014). The active subspace method was proposed to reduce the  
473 dimension of a complex hydrological model dedicated to karst hydrology (Bittner et al., 2020a) and  
474 could be applied to assess the improvement due to the increased level of hydrological model complexity.  
475 The latter can consist of considering a pseudo-distributed recharge, a threshold effect (with activation  
476 of fluxes routine) or even dividing the baseflow compartment into several flow dynamics with potential  
477 exchanges. Finally, assessing a pseudo-distributed recharge in lumped parameter modeling in karst  
478 hydrology is interesting for further research when assessing the combined impact of climate and LCLU  
479 changes on karst systems.

## 480 **5 Conclusion**

481 The study focuses on the future development of the Mediterranean karst spring discharge for various  
482 climate and anthropogenic pressure changes. The results in this study mainly focus on the relative impact  
483 of climate change and anthropogenic forcing respectively. The main result of the study is that climate  
484 change has a major effect on the future evolution of the studied Mediterranean karst spring's discharge.  
485 Groundwater abstraction constitutes a secondary but non-negligible factor which contributes to the dry-

486 up of the spring. If groundwater abstraction is increased, its contributions may rise up to 25% of the  
487 annual spring discharge decrease, and up to 40% of the monthly spring discharge during the summer  
488 period. This may indicate that the system is not overexploited but still highly sensible to groundwater  
489 extraction.

490 Finally, the workflow proposed in this study consists of a multiple scenario testing procedure allowing  
491 to account for uncertainties in climate model simulations and hydrological model conceptualizations. It  
492 may be a helpful tool to assess groundwater variability in karst systems under active management and  
493 changing environmental conditions, while simultaneously provide valuable information for stakeholders  
494 and decision-makers for a sustainable freshwater supply in karst regions.

## 495 **Acknowledgements**

496 The authors would like to thank the French Karst National Observatory Service (SNO KARST) initiative  
497 at the INSU/CNRS which aims to strengthen dissemination of knowledge and promotes cross-  
498 disciplinarily research on karst systems at the national scale, for their support on the use of the KarstMod  
499 model. The authors would also like to thank Météo-France for providing the meteorological data as well  
500 as the EURO-CORDEX initiative for providing the RCM/GCM simulations used in this study through  
501 the ESGF platform. The authors appreciate the valuable help of Rémi Muller and Lucie Martin during  
502 fieldwork at Oeillal spring. Daniel Bittner further acknowledges the support by the Deutsche  
503 Forschungsgemeinschaft (DFG) in the framework of the ROCKAT project (CH 981/6-1).

## 504 **Funding**

505 The present study and the field monitoring near the Oeillal spring was funded by ORANO Malvesi.

## 506 **Credit author statement**

507 **Vianney Sivel**: Conceptualization, Methodology, Software, Formal analysis, Writing- Original draft  
508 preparation, **Hervé Jourde**: Supervision, Project administration, Funding acquisition, Reviewing and  
509 Editing, **Daniel Bittner**: Software, Reviewing and Editing, **Naomi Mazzilli**: Software, Reviewing and  
510 Editing, **Yves Trambly**: Data Curation, Reviewing and Editing

511 **Appendix A**

512 The model is based on a structure available within the KarstMod modeling platform (Jourde et al., 2015;  
 513 Mazzilli et al., 2019). The model consists of two interconnected compartments: a compartment E (higher  
 514 level) and a compartment M (lower level) for which the mass-balance equations provided by Mazzilli  
 515 et al. (2019) are applied.

$$\frac{dE}{dt} = P - ET - Q_{EM} - Q_{ES} \text{ if } E \geq 0 \quad (\text{A.1})$$

$$\frac{dE}{dt} = P - ET \text{ if } E_{min} < E < 0 \quad (\text{A.2})$$

$$\frac{dM}{dt} = Q_{EM} - Q_{MS} - Q_{bM} - Q_{rM} \quad (\text{A.3})$$

516 where:  $E$  and  $M$  refer to the water levels in compartments E and M respectively,  $E_{min}$  is the minimum  
 517 water level in compartment E,  $P$  is the precipitation rate,  $ET$  is the evapotranspiration rate. Note that  $P$   
 518 and  $ET$  only affect compartment E (upper level). When the water level in E is greater than  $E_{min}$ , the water  
 519 flows either towards the lower compartment M (discharge  $Q_{EM}$ ) or directly to the outlet (discharge  $Q_{ES}$ ).  
 520 The compartment M is characterized by a transfer function with an infinite characteristic time (Guinot  
 521 et al., 2015). The unit response  $\omega(t)$  of the compartment M is defined as:

$$\omega(t) = \frac{\alpha_M \times \tau_M^{\alpha_M}}{(\tau_A + t)^{\alpha_M + 1}} \quad (\text{A.4})$$

522 where  $\alpha_M \in (0,1)$  is an exponent and  $\tau_A$  is a time scale. The outflowing discharge  $Q_{bM}$  from the  
 523 compartment M is related to the inflow rate  $R = Q_{EM}$  by the convolution product:

$$Q_{bM} = R \circledast \omega(t) \quad (\text{A.5})$$

524 The convolution kernel is approximated with a set of local operators run in parallel (Guinot et al., 2015).  
 525 The compartment M is split into  $n$  sub-compartments with linear laws. The water level  $M(t)$  in  
 526 compartment M is equal to the weighted sum of water levels  $M_i(t)$  in the  $n$  sub-compartments. The  
 527 outflowing discharge rate  $Q_{bM}$  from compartment M equals the weighted sum of the specific outflow  
 528 rates  $Q_{bM_i}$  from the  $n$  sub-compartments:

$$M(t) = \sum_{i=1}^n \theta_i M_i(t) \quad (\text{A.6})$$

$$Q_{bM}(t) = \sum_{i=1}^n \theta_i Q_{bM_i}(t) \quad (\text{A.7})$$

$$\sum_{i=1}^n \theta_i = 1 \quad (\text{A.8})$$

529 An upper threshold  $h_{max}^M$  is set for the depth in the sub-compartments. When the water level  $M(t)$   
530 becomes greater than  $h_{max}^M$ , the  $i^{\text{th}}$  sub-compartment is bypassed and the corresponding overflow  $Q_{rM_i}$   
531 is routed directly to the loss. Such rapid overflow may occur even though the average water level  $M(t)$   
532 is below the upper threshold  $h_{max}^M$ . Indeed, some sub-compartments may pass the  $h_{max}^M$  threshold while  
533 the weighted sum  $M(t)$  stays below  $h_{max}^M$ . The total overflow  $Q_{rM}$  is equal to the weighted sum of the  
534 specific outflow rates  $Q_{rM_i}$  from the  $n$  sub-compartments:

$$Q_{rM}(t) = \sum_{i=1}^n \theta_i Q_{rM_i}(t) \quad (9)$$

535 where the condition on  $\theta_i$  in Eq. A.8 is still applicable.

536 **Appendix B**

537 In a LuKARS model, areas with homogeneous infiltration conditions are implemented as distinct  
 538 hydrological response units, called hydrotopes. A hydrotope is analogous to a bucket that has three  
 539 discharge components: the quickflow component ( $Q_{hyd}$  [ $L^3T^{-1}$ ]), a secondary spring discharge ( $Q_{sec}$   
 540 [ $L^3T^{-1}$ ]), and the recharge ( $Q_{is}$  [ $L^3T^{-1}$ ]).  $Q_{hyd}$  is considered a hydrotope-specific quickflow occurring in  
 541 preferential flow paths (e.g. subsurface conduits). The quickflow bypasses the baseflow storage B and  
 542 is directly transferred to the spring outlet. The quickflow starts, once a hydrotope-specific storage  
 543 threshold ( $E_{max}$ ) has been reached and stops after the hydrotope storage falls below a lower storage  
 544 threshold ( $E_{min}$ ).  $Q_{sec}$  integrates all flow components that do not arrive at the simulated karst spring  
 545 and that are transferred outside the regarded recharge area, i.e. secondary spring discharge and overland  
 546 flow (Tritz et al., 2011).  $Q_{is}$  is the discharge from one hydrotope to the underlying baseflow storage B  
 547 that represents the process of groundwater recharge. Each hydrotope has 7 physical parameters, with  
 548 length units  $L$  and time units  $T$ , that are as follows:

- 549 •  $k_{hyd}$  [ $L^2T^{-1}$ ] is the discharge parameter for  $Q_{hyd}$ ,
- 550 •  $E_{min}$  [L] is the minimum storage capacity of a hydrotope,
- 551 •  $E_{max}$  [L] is the maximum storage capacity of a hydrotope,
- 552 •  $\alpha$  [-] is the hydrotope-specific quickflow exponent,
- 553 •  $k_{is}$  [ $LT^{-1}$ ] is the discharge parameter for  $Q_{is}$ ,
- 554 •  $k_{sec}$  [ $LT^{-1}$ ] is the discharge parameter for  $Q_{sec}$ ,
- 555 •  $E_{sec}$  [L] is the activation level for  $Q_{sec}$

556 Following the conceptual sketch from Bittner et al., (2018), the model solves the following discrete  
 557 balance equations for each hydrotope  $i$  and for each time step  $n$  :

$$E_{i,n+1} = \max \left[ 0, E_{i,n} + \left( S_{i,n} - \frac{Q_{hyd,i,n} + Q_{sec,i,b} + Q_{is,i,n}}{a_i} \right) \Delta t \right] \quad (B.1)$$

558 Where  $E_i$  indicates the water level [L] in hydrotope  $i$ .  $S_i$  is the hydrotope-specific sink and source term  
 559 as a mass balance of precipitation, evapotranspiration, and interception. Then, evapotranspiration is

560 considered using the formula from Oudin et al., (2005).  $Q_{hyd,i}$  [ $L^3T^{-1}$ ] represents the quickflow  
 561 component (e.g. conduit flow),  $Q_{sec,i}$  [ $L^2T^{-1}$ ] refers to the secondary spring discharge, and  $Q_{is,i}$  [ $L^2T^{-1}$ ]  
 562 is the groundwater recharge. The absolute area covered by a respective hydrotope is given by  $a_i$  [ $L^2$ ].

$$E_{b,n+1} = \max \left[ 0, E_{b,n} + \left( \frac{\sum(Q_{is,i,n}) - Q_{b,n} - Q_{pumpB,n}}{A} \right) \Delta t \right] \quad (B.2)$$

563 is the balance equation for the baseflow storage B, where  $E_b$  indicates the water level [L] in the baseflow  
 564 storage,  $\sum(Q_{is,i,n})$  [ $L^3T^{-1}$ ] indicates the cumulative flows from all hydrotopes to the baseflow storage,  
 565  $Q_b$  [ $L^3T^{-1}$ ] indicates water that is transferred from the storage B to the spring, hence simulates the  
 566 baseflow contribution from the phreatic aquifer system to the spring discharge, and  $Q_{pumpB}$  [ $L^3T^{-1}$ ]  
 567 indicates the groundwater abstraction in the aquifer. The variable  $A$  [ $L^2$ ] stands for the entire recharge  
 568 area. The discharge terms are computed as follows:

$$Q_{hyd,i,n} = a_i \frac{k_{hyd,i}}{l_{hyd,i}} \varepsilon_n \left[ \frac{\max(0, E_{i,n} - E_{min,i})}{E_{max,i} - E_{min,i}} \right] \alpha_i \quad (B.3)$$

$$Q_{sec,i,n} = a_i k_{sec,i} \max(0, E_{i,n} - E_{sec,i}) \quad (B.4)$$

$$Q_{is,i,n} = a_i k_{is,i} E_{i,n} \quad (B.5)$$

$$Q_{b,n} = \begin{cases} [k_b * E_{b,n} + 0.2 * k_b * (E_{b,n} - ceil_B)] * A \text{ if } E_{b,n} \geq ceil_B \\ k_b * E_{b,n} * A \text{ if } E_{b,n} < ceil_B \end{cases} \quad (B.6)$$

569  $E_{max,i}$  [L] and  $E_{min,i}$  [L] represent the upper and lower storage thresholds of the hydrotope  $i$ .  $E_{sec,i}$  [L]  
 570 is the hydrotope-specific activation level for a secondary spring discharge.  $k_{sec,i}$  [ $LT^{-1}$ ],  $k_{is,i}$  [ $LT^{-1}$ ] and  
 571  $k_b$  [ $LT^{-1}$ ] are the specific discharge parameters for  $Q_{sec,i}$  [ $L^3T^{-1}$ ],  $Q_{is,i}$  [ $L^3T^{-1}$ ] and  $Q_b$  [ $L^3T^{-1}$ ],  
 572 respectively.  $k_{hyd,i}$  [ $L^2T^{-1}$ ] represents the specific discharge parameter for the quickflow of a hydrotope  
 573 and  $l_{hyd,i}$  [L] is the mean distance of hydrotope  $i$  to the adjacent spring, thus accounting for the relative  
 574 location of the same hydrotope types in a specific recharge area. The ratio between  $k_{hyd,i}$  and  $l_{hyd,i}$   
 575 represents the hydrotope discharge coefficient and  $\alpha_i$  is a hydrotope-specific exponent of the quickflow.  
 576 The dimensionless connectivity/activation indicator  $\varepsilon$  is defined as follows:

$$\varepsilon_{n+1} = 0 \text{ if } \{\varepsilon_n = 0 \wedge \varepsilon_{i,n+1} < E_{max,i} \vee \varepsilon_n = 1 \wedge \varepsilon_{i,n+1} \leq E_{min,i}\} \quad (\text{B.7})$$

$$\varepsilon_{n+1} = 1 \text{ if } \{\varepsilon_n = 0 \wedge \varepsilon_{i,n+1} \geq E_{max,i} \vee \varepsilon_n = 1 \wedge \varepsilon_{i,n+1} > E_{min,i}\} \quad (\text{B.8})$$

577 To account for groundwater abstraction, the original equation for the baseflow compartment in the  
 578 LuKARS model is modified as follows:

$$B_{n+1} = \max \left[ 0, B_n + \left( \frac{Q_{is,n} - Q_{b,n} - Q_{pumpB}}{A} \right) * \Delta t \right] \quad (\text{B.9})$$

$$Q_{b,n} = \begin{cases} \left[ k_{b_{down}} * E_{b,n} + k_{b_{up}} * (E_{b,n} - threshold_B) \right] * A \text{ if } E_{b,n} \geq threshold_B \\ k_{b_{down}} * E_{b,n} * A \text{ if } E_{b,n} < threshold_B \end{cases} \quad (\text{B.10})$$

579 where  $B_n$  is the water level [L] in the baseflow compartment at the time step  $n$ ,  $Q_{is,n}$  is the total flow  
 580 from all hydrotropes to the baseflow compartment [ $L^3T^{-1}$ ],  $Q_{b_{down}}$  is the flow from the linear baseflow  
 581 compartment to the spring [ $L^3T^{-1}$ ],  $Q_{b_{up}}$  is the flow from the linear baseflow compartment corresponding  
 582 to the overflow when the water level  $B_n \geq threshold_B$ ,  $Q_{pumpB}$  is the groundwater abstraction  
 583 discharge [ $L^3T^{-1}$ ],  $A$  is the total recharge area [ $L^2$ ].

584 **References**

- 585 Bakalowicz, M., 2015. Karst and karst groundwater resources in the Mediterranean. *Environ Earth Sci*  
 586 74, 5–14. <https://doi.org/10.1007/s12665-015-4239-4>
- 587 Bendtsen, C., 2012. pso: Particle Swarm Optimization.
- 588 Bittner, D., Narany, T.S., Kohl, B., Disse, M., Chiogna, G., 2018. Modeling the hydrological impact of  
 589 land use change in a dolomite-dominated karst system. *Journal of Hydrology* 567, 267–279.  
 590 <https://doi.org/10.1016/j.jhydrol.2018.10.017>
- 591 Bittner, D., Parente, M.T., Mattis, S., Wohlmuth, B., Chiogna, G., 2020a. Identifying relevant  
 592 hydrological and catchment properties in active subspaces: An inference study of a lumped karst  
 593 aquifer model. *Advances in Water Resources* 135, 103472.  
 594 <https://doi.org/10.1016/j.advwatres.2019.103472>
- 595 Bittner, D., Rychlik, A., Klöffel, T., Leuteritz, A., Disse, M., Chiogna, G., 2020b. A GIS-based model  
 596 for simulating the hydrological effects of land use changes on karst systems – The integration  
 597 of the LuKARS model into FREEWAT. *Environmental Modelling & Software* 127, 104682.  
 598 <https://doi.org/10.1016/j.envsoft.2020.104682>
- 599 Brohan, P., Kennedy, J.J., Harris, I., Tett, S.F.B., Jones, P.D., 2006. Uncertainty estimates in regional  
 600 and global observed temperature changes: A new data set from 1850. *Journal of Geophysical*  
 601 *Research: Atmospheres* 111. <https://doi.org/10.1029/2005JD006548>
- 602 Bussotti, F., Ferrini, F., Pollastrini, M., Fini, A., 2014. The challenge of Mediterranean sclerophyllous  
 603 vegetation under climate change: From acclimation to adaptation. *Environmental and*  
 604 *Experimental Botany, Response to abiotic stresses of plants of Mediterranean-type ecosystems*  
 605 103, 80–98. <https://doi.org/10.1016/j.envexpbot.2013.09.013>
- 606 Chang, Y., Wu, J., Jiang, G., Kang, Z., 2017. Identification of the dominant hydrological process and  
 607 appropriate model structure of a karst catchment through stepwise simplification of a complex  
 608 conceptual model. *Journal of Hydrology* 548, 75–87.  
 609 <https://doi.org/10.1016/j.jhydrol.2017.02.050>
- 610 Charlier, J.-B., Ladouche, B., Maréchal, J.-C., 2015. Identifying the impact of climate and anthropic  
 611 pressures on karst aquifers using wavelet analysis. *Journal of Hydrology* 523, 610–623.  
 612 <https://doi.org/10.1016/j.jhydrol.2015.02.003>
- 613 Clauzon, V., Mayolle, S., Leonardi, V., Brunet, P., Soliva, R., Marchand, P., Massonnat, G., Rolando,  
 614 J.-P., Pistre, S., 2020. Fault zones in limestones: impact on karstogenesis and groundwater flow  
 615 (Lez aquifer, southern France). *Hydrogeol J.* <https://doi.org/10.1007/s10040-020-02189-9>
- 616 Cosandey, C., Andréassian, V., Martin, C., Didon-Lescot, J.F., Lavabre, J., Folton, N., Mathys, N.,  
 617 Richard, D., 2005. The hydrological impact of the mediterranean forest: a review of French  
 618 research. *Journal of Hydrology* 301, 235–249. <https://doi.org/10.1016/j.jhydrol.2004.06.040>
- 619 Dausse, A., Leonardi, V., Jourde, H., 2019. Hydraulic characterization and identification of flow-bearing  
 620 structures based on multi-scale investigations applied to the Lez karst aquifer. *Journal of*  
 621 *Hydrology: Regional Studies* 26, 100627. <https://doi.org/10.1016/j.ejrh.2019.100627>
- 622 Delrieu, G., Boudevillain, B., Nicol, J., Chapon, B., Kirstetter, P.-E., Andrieu, H., Faure, D., 2009.  
 623 Bollène-2002 Experiment: Radar Quantitative Precipitation Estimation in the Cévennes–  
 624 Vivarais Region, France. *Journal of Applied Meteorology and Climatology* 48, 1422–1447.  
 625 <https://doi.org/10.1175/2008JAMC1987.1>
- 626 Déqué, M., 2007. Frequency of precipitation and temperature extremes over France in an anthropogenic  
 627 scenario: Model results and statistical correction according to observed values. *Global and*  
 628 *Planetary Change, Extreme Climatic Events* 57, 16–26.  
 629 <https://doi.org/10.1016/j.gloplacha.2006.11.030>

- 630 Devia, G.K., Ganasri, B.P., Dwarakish, G.S., 2015. A Review on Hydrological Models. Aquatic  
631 Procedia, INTERNATIONAL CONFERENCE ON WATER RESOURCES, COASTAL AND  
632 OCEAN ENGINEERING (ICWRCOE'15) 4, 1001–1007.  
633 <https://doi.org/10.1016/j.aqpro.2015.02.126>
- 634 Diffenbaugh, N.S., Giorgi, F., 2012. Climate change hotspots in the CMIP5 global climate model  
635 ensemble. Climatic Change 114, 813–822. <https://doi.org/10.1007/s10584-012-0570-x>
- 636 Doummar, J., Hassan Kassem, A., Gurdak, J.J., 2018. Impact of historic and future climate on spring  
637 recharge and discharge based on an integrated numerical modelling approach: Application on a  
638 snow-governed semi-arid karst catchment area. Journal of Hydrology 565, 636–649.  
639 <https://doi.org/10.1016/j.jhydrol.2018.08.062>
- 640 Dubois, E., Doummar, J., Pistre, S., Larocque, M., 2020. Calibration of a lumped karst system model  
641 and application to the Qachqouch karst spring (Lebanon) under climate change conditions.  
642 Hydrology and Earth System Sciences 24, 4275–4290. [https://doi.org/10.5194/hess-24-4275-](https://doi.org/10.5194/hess-24-4275-2020)  
643 2020
- 644 ENTECH, 2016. Déclaration au titre des articles L.214-1 à L.314-6 du Code de l'Environnement - 3.1  
645 Présentation du captage (Déclaration d'Utilité Publique). Département de l'Aude , Le Grand  
646 Narbonne Communauté d'Agglomération, Narbonne.
- 647 European Environment Agency & Copernicus Land Service., n.d. Corine Land Cover 2018 [WWW  
648 Document]. URL <https://land.copernicus.eu/pan-european/corine-land-cover/clc2018>  
649 (accessed 10.19.20).
- 650 Fiorillo, F., Guadagno, F.M., 2012. Long karst spring discharge time series and droughts occurrence in  
651 Southern Italy. Environ Earth Sci 65, 2273–2283. <https://doi.org/10.1007/s12665-011-1495-9>
- 652 Fleury, P., Plagnes, V., Bakalowicz, M., 2007. Modelling of the functioning of karst aquifers with a  
653 reservoir model: Application to Fontaine de Vaucluse (South of France). Journal of Hydrology  
654 345, 38–49. <https://doi.org/10.1016/j.jhydrol.2007.07.014>
- 655 García-Ruiz, J.M., López-Moreno, J.I., Vicente-Serrano, S.M., Lasanta-Martínez, T., Beguería, S.,  
656 2011. Mediterranean water resources in a global change scenario. Earth-Science Reviews 105,  
657 121–139. <https://doi.org/10.1016/j.earscirev.2011.01.006>
- 658 Giorgi, F., 2006. Climate change hot-spots. Geophysical Research Letters 33.  
659 <https://doi.org/10.1029/2006GL025734>
- 660 Gleeson, T., Wada, Y., Bierkens, M.F.P., van Beek, L.P.H., 2012. Water balance of global aquifers  
661 revealed by groundwater footprint. Nature 488, 197–200. <https://doi.org/10.1038/nature11295>
- 662 Goldscheider, N., Chen, Z., Auler, A.S., Bakalowicz, M., Broda, S., Drew, D., Hartmann, J., Jiang, G.,  
663 Moosdorf, N., Stevanovic, Z., Veni, G., 2020. Global distribution of carbonate rocks and karst  
664 water resources. Hydrogeol J. <https://doi.org/10.1007/s10040-020-02139-5>
- 665 Grillakis, M.G., Koutroulis, A.G., Tsanis, I.K., 2013. Multisegment statistical bias correction of daily  
666 GCM precipitation output. Journal of Geophysical Research: Atmospheres 118, 3150–3162.  
667 <https://doi.org/10.1002/jgrd.50323>
- 668 Guinot, V., Savéan, M., Jourde, H., Neppel, L., 2015. Conceptual rainfall–runoff model with a two-  
669 parameter, infinite characteristic time transfer function. Hydrological Processes 29, 4756–4778.  
670 <https://doi.org/10.1002/hyp.10523>
- 671 Gupta, H.V., Kling, H., Yilmaz, K.K., Martinez, G.F., 2009. Decomposition of the mean squared error  
672 and NSE performance criteria: Implications for improving hydrological modelling. Journal of  
673 Hydrology 377, 80–91. <https://doi.org/10.1016/j.jhydrol.2009.08.003>
- 674 Hartmann, A., 2018. Experiences in calibrating and evaluating lumped karst hydrological models.  
675 Geological Society, London, Special Publications 466, 331–340.  
676 <https://doi.org/10.1144/SP466.18>

- 677 Hartmann, A., Goldscheider, N., Wagener, T., Lange, J., Weiler, M., 2014. Karst water resources in a  
678 changing world: Review of hydrological modeling approaches. *Rev. Geophys.* 52, 218–242.  
679 <https://doi.org/10.1002/2013RG000443>
- 680 Hartmann, Andreas, Lange, J., Vivó Aguado, À., Mizyed, N., Smiatek, G., Kunstmann, H., 2012. A  
681 multi-model approach for improved simulations of future water availability at a large Eastern  
682 Mediterranean karst spring. *Journal of Hydrology* 468–469, 130–138.  
683 <https://doi.org/10.1016/j.jhydrol.2012.08.024>
- 684 Hartmann, A., Lange, J., Weiler, M., Arbel, Y., Greenbaum, N., 2012. A new approach to model the  
685 spatial and temporal variability of recharge to karst aquifers. *Hydrology and Earth System  
686 Sciences* 16, 2219–2231. <https://doi.org/10.5194/hess-16-2219-2012>
- 687 Jacob, D., Petersen, J., Eggert, B., Alias, A., Christensen, O.B., Bouwer, L.M., Braun, A., Colette, A.,  
688 Déqué, M., Georgievski, G., Georgopoulou, E., Gobiet, A., Menut, L., Nikulin, G., Haensler,  
689 A., Hempelmann, N., Jones, C., Keuler, K., Kovats, S., Kröner, N., Kotlarski, S., Kriegsmann,  
690 A., Martin, E., van Meijgaard, E., Moseley, C., Pfeifer, S., Preuschmann, S., Radermacher, C.,  
691 Radtke, K., Rechid, D., Rounsevell, M., Samuelsson, P., Somot, S., Soussana, J.-F., Teichmann,  
692 C., Valentini, R., Vautard, R., Weber, B., Yiou, P., 2014. EURO-CORDEX: new high-  
693 resolution climate change projections for European impact research. *Reg Environ Change* 14,  
694 563–578. <https://doi.org/10.1007/s10113-013-0499-2>
- 695 Jacob, D., Teichmann, C., Sobolowski, S., Katragkou, E., Anders, I., Belda, M., Benestad, R., Boberg,  
696 F., Buonomo, E., Cardoso, R.M., Casanueva, A., Christensen, O.B., Christensen, J.H., Coppola,  
697 E., De Cruz, L., Davin, E.L., Dobler, A., Domínguez, M., Fealy, R., Fernandez, J., Gaertner,  
698 M.A., García-Díez, M., Giorgi, F., Gobiet, A., Goergen, K., Gómez-Navarro, J.J., Alemán,  
699 J.J.G., Gutiérrez, C., Gutiérrez, J.M., Güttler, I., Haensler, A., Halenka, T., Jerez, S., Jiménez-  
700 Guerrero, P., Jones, R.G., Keuler, K., Kjellström, E., Knist, S., Kotlarski, S., Maraun, D., van  
701 Meijgaard, E., Mercogliano, P., Montávez, J.P., Navarra, A., Nikulin, G., de Noblet-Ducoudré,  
702 N., Panitz, H.-J., Pfeifer, S., Piazza, M., Pichelli, E., Pietikäinen, J.-P., Prein, A.F.,  
703 Preuschmann, S., Rechid, D., Rockel, B., Romera, R., Sánchez, E., Sieck, K., Soares, P.M.M.,  
704 Somot, S., Srncic, L., Sørland, S.L., Termonia, P., Truhetz, H., Vautard, R., Warrach-Sagi, K.,  
705 Wulfmeyer, V., 2020. Regional climate downscaling over Europe: perspectives from the  
706 EURO-CORDEX community. *Reg Environ Change* 20, 51. <https://doi.org/10.1007/s10113-020-01606-9>
- 707
- 708 Jiang, T., Chen, Y.D., Xu, C., Chen, Xiaohong, Chen, Xi, Singh, V.P., 2007. Comparison of  
709 hydrological impacts of climate change simulated by six hydrological models in the Dongjiang  
710 Basin, South China. *Journal of Hydrology* 336, 316–333.  
711 <https://doi.org/10.1016/j.jhydrol.2007.01.010>
- 712 Jones, R.N., Chiew, F.H.S., Boughton, W.C., Zhang, L., 2006. Estimating the sensitivity of mean annual  
713 runoff to climate change using selected hydrological models. *Advances in Water Resources* 29,  
714 1419–1429. <https://doi.org/10.1016/j.advwatres.2005.11.001>
- 715 Jourde, H., Lafare, A., Mazzilli, N., Belaud, G., Neppel, L., Dörfliger, N., Cernesson, F., 2014. Flash  
716 flood mitigation as a positive consequence of anthropogenic forcing on the groundwater  
717 resource in a karst catchment. *Environ Earth Sci* 71, 573–583. <https://doi.org/10.1007/s12665-013-2678-3>
- 718
- 719 Jourde, H., Mazzilli, N., Lecoq, N., Arfib, B., Bertin, D., 2015. KARSTMOD: A Generic Modular  
720 Reservoir Model Dedicated to Spring Discharge Modeling and Hydrodynamic Analysis in  
721 Karst, in: Andreo, B., Carrasco, F., Durán, J.J., Jiménez, P., LaMoreaux, J.W. (Eds.),  
722 Hydrogeological and Environmental Investigations in Karst Systems. Springer Berlin  
723 Heidelberg, Berlin, Heidelberg, pp. 339–344. [https://doi.org/10.1007/978-3-642-17435-3\\_38](https://doi.org/10.1007/978-3-642-17435-3_38)
- 724 Kazakis, N., Chalikakis, K., Mazzilli, N., Ollivier, C., Manakos, A., Voudouris, K., 2018. Management  
725 and research strategies of karst aquifers in Greece: Literature overview and exemplification  
726 based on hydrodynamic modelling and vulnerability assessment of a strategic karst aquifer.

- 727 Science of The Total Environment 643, 592–609.  
728 <https://doi.org/10.1016/j.scitotenv.2018.06.184>
- 729 Klaas, D.K.S.Y., Imteaz, M.A., Sudiayem, I., Klaas, E.M.E., Klaas, E.C.M., 2020. Assessing climate  
730 changes impacts on tropical karst catchment: Implications on groundwater resource  
731 sustainability and management strategies. *Journal of Hydrology* 582, 124426.  
732 <https://doi.org/10.1016/j.jhydrol.2019.124426>
- 733 Klausmeyer, K.R., Shaw, M.R., 2009. Climate Change, Habitat Loss, Protected Areas and the Climate  
734 Adaptation Potential of Species in Mediterranean Ecosystems Worldwide. *PLOS ONE* 4,  
735 e6392. <https://doi.org/10.1371/journal.pone.0006392>
- 736 Ladouche, B., Marechal, J.-C., Dorfliger, N., 2014. Semi-distributed lumped model of a karst system  
737 under active management. *Journal of Hydrology* 509, 215–230.  
738 <https://doi.org/10.1016/j.jhydrol.2013.11.017>
- 739 Lavorel, S., Canadell, J., Rambal, S., Terradas, J., 1998. Mediterranean terrestrial ecosystems: research  
740 priorities on global change effects. *Global Ecology & Biogeography Letters* 7, 157–166.  
741 <https://doi.org/10.1046/j.1466-822X.1998.00277.x>
- 742 Lelièvre, F., Sala, S., Volaire, F., 2010. Climate change at the temperate-Mediterranean interface in  
743 southern France and impacts on grasslands production, in: *The Contributions of Grasslands to  
744 the Conservation of Mediterranean Biodiversity*. Zaragoza : CIHEAM / CIBIO / FAO / SEEP,  
745 *Options Méditerranéennes : Série A. Séminaires Méditerranéens*. pp. 187–192.
- 746 Lespinas, F., Ludwig, W., Heussner, S., 2010. Impact of recent climate change on the hydrology of  
747 coastal Mediterranean rivers in Southern France. *Climatic Change* 99, 425–456.  
748 <https://doi.org/10.1007/s10584-009-9668-1>
- 749 Llorens, P., Domingo, F., 2007. Rainfall partitioning by vegetation under Mediterranean conditions. A  
750 review of studies in Europe. *Journal of Hydrology* 335, 37–54.  
751 <https://doi.org/10.1016/j.jhydrol.2006.10.032>
- 752 Loáiciga, H.A., Maidment, D.R., Valdes, J.B., 2000. Climate-change impacts in a regional karst aquifer,  
753 Texas, USA. *Journal of Hydrology* 227, 173–194. [https://doi.org/10.1016/S0022-1694\(99\)00179-1](https://doi.org/10.1016/S0022-1694(99)00179-1)
- 755 Mazzilli, N., Guinot, V., Jourde, H., Lecoq, N., Labat, D., Arfib, B., Baudement, C., Danquigny, C., Dal  
756 Soglio, L., Bertin, D., 2019. KarstMod: A modelling platform for rainfall - discharge analysis  
757 and modelling dedicated to karst systems. *Environmental Modelling & Software* 122, 103927.  
758 <https://doi.org/10.1016/j.envsoft.2017.03.015>
- 759 McSweeney, C.F., Jones, R.G., Lee, R.W., Rowell, D.P., 2015. Selecting CMIP5 GCMs for  
760 downscaling over multiple regions. *Clim Dyn* 44, 3237–3260. <https://doi.org/10.1007/s00382-014-2418-8>
- 762 Moisselin, J.-M., Schneider, M., Canellas, C., 2002. Les changements climatiques en France au XX<sup>e</sup>  
763 siècle. Etude des longues séries homogénéisées de données de température et de précipitations.  
764 *Météorologie* 8, 45. <https://doi.org/10.4267/2042/36233>
- 765 Nerantzaki, S.D., Nikolaidis, N.P., 2020. The response of three Mediterranean karst springs to drought  
766 and the impact of climate change. *Journal of Hydrology* 591, 125296.  
767 <https://doi.org/10.1016/j.jhydrol.2020.125296>
- 768 Ollivier, C., Mazzilli, N., Oliosio, A., Chalikakis, K., Carrière, S.D., Danquigny, C., Emblanch, C., 2020.  
769 Karst recharge-discharge semi distributed model to assess spatial variability of flows. *Science  
770 of The Total Environment* 703, 134368. <https://doi.org/10.1016/j.scitotenv.2019.134368>
- 771 Oudin, L., Hervieu, F., Michel, C., Perrin, C., Andréassian, V., Anctil, F., Loumagne, C., 2005. Which  
772 potential evapotranspiration input for a lumped rainfall–runoff model? *Journal of Hydrology*  
773 303, 290–306. <https://doi.org/10.1016/j.jhydrol.2004.08.026>

- 774 Perrin, C., Michel, C., Andréassian, V., 2001. Does a large number of parameters enhance model  
775 performance? Comparative assessment of common catchment model structures on 429  
776 catchments. *Journal of Hydrology* 242, 275–301. [https://doi.org/10.1016/S0022-](https://doi.org/10.1016/S0022-1694(00)00393-0)  
777 1694(00)00393-0
- 778 R Core Team, 2013. R: A language and environment for statistical computing. R Foundation for  
779 Statistical Computing. Vienna, Austria.
- 780 Refsgaard, J.C., Henriksen, H.J., 2004. Modelling guidelines—terminology and guiding principles.  
781 *Advances in Water Resources* 27, 71–82. <https://doi.org/10.1016/j.advwatres.2003.08.006>
- 782 SAFEGE, 2019. Reconnaissances hydrogéologiques dans le cadre du PNGMDR sur le site de Malvési  
783 à Narbonne (11). Suivis de la source de l’Oeillal et des piézomètres FR1, FR2, FR3, K1 et K2.
- 784 Sapač, K., Medved, A., Rusjan, S., Bezak, N., 2019. Investigation of Low- and High-Flow  
785 Characteristics of Karst Catchments under Climate Change. *Water* 11, 925.  
786 <https://doi.org/10.3390/w11050925>
- 787 Sivellev, V., Jourde, H., 2020. A methodology for the assessment of groundwater resource variability in  
788 karst catchments with sparse temporal measurements. *Hydrogeol J.*  
789 <https://doi.org/10.1007/s10040-020-02239-2>
- 790 Smiatek, G., Kaspar, S., Kunstmann, H., 2013. Hydrological Climate Change Impact Analysis for the  
791 Figh Spring near Damascus, Syria. *Journal of Hydrometeorology* 14, 577–593.  
792 <https://doi.org/10.1175/JHM-D-12-065.1>
- 793 Stefano, L.D., Duncan, J., Dinar, S., Stahl, K., Strzepek, K.M., Wolf, A.T., 2012. Climate change and  
794 the institutional resilience of international river basins: *Journal of Peace Research.*  
795 <https://doi.org/10.1177/0022343311427416>
- 796 Stevanović, Z., 2019. Karst Aquifers in the Arid World of Africa and the Middle East: Sustainability or  
797 Humanity?, in: Younos, T., Schreiber, M., Kosič Ficco, K. (Eds.), *Karst Water Environment:*  
798 *Advances in Research, Management and Policy*, The Handbook of Environmental Chemistry.  
799 Springer International Publishing, Cham, pp. 1–43. [https://doi.org/10.1007/978-3-319-77368-](https://doi.org/10.1007/978-3-319-77368-1_1)  
800 1\_1
- 801 Stevanović, Z., 2018. Global distribution and use of water from karst aquifers. Geological Society,  
802 London, Special Publications 466, 217–236. <https://doi.org/10.1144/SP466.17>
- 803 Stevanovic, Z., 2010. Case Study: Major springs of southeastern Europe and their Utilization, in: Kresic,  
804 N., Stevanovic, Z. (Eds.), *Groundwater Hydrology of Springs*. Butterworth-Heinemann,  
805 Boston, pp. 389–410. <https://doi.org/10.1016/B978-1-85617-502-9.00010-4>
- 806 Taylor, K.E., Stouffer, R.J., Meehl, G.A., 2012. An Overview of CMIP5 and the Experiment Design.  
807 *Bull. Amer. Meteor. Soc.* 93, 485–498. <https://doi.org/10.1175/BAMS-D-11-00094.1>
- 808 Taylor, R.G., Scanlon, B., Döll, P., Rodell, M., van Beek, R., Wada, Y., Longuevergne, L., Leblanc, M.,  
809 Famiglietti, J.S., Edmunds, M., Konikow, L., Green, T.R., Chen, J., Taniguchi, M., Bierkens,  
810 M.F.P., MacDonald, A., Fan, Y., Maxwell, R.M., Yechieli, Y., Gurdak, J.J., Allen, D.M.,  
811 Shamsudduha, M., Hiscock, K., Yeh, P.J.-F., Holman, I., Treidel, H., 2013. Ground water and  
812 climate change. *Nature Climate Change* 3, 322–329. <https://doi.org/10.1038/nclimate1744>
- 813 Trambly, Y., Koutroulis, A., Samaniego, L., Vicente-Serrano, S.M., Volaire, F., Boone, A., Le Page,  
814 M., Llasat, M.C., Albergel, C., Burak, S., Cailleret, M., Kalin, K.C., Davi, H., Dupuy, J.-L.,  
815 Greve, P., Grillakis, M., Hanich, L., Jarlan, L., Martin-StPaul, N., Martínez-Vilalta, J., Mouillot,  
816 F., Pulido-Velazquez, D., Quintana-Seguí, P., Renard, D., Turco, M., Türkeş, M., Trigo, R.,  
817 Vidal, J.-P., Vilagrosa, A., Zribi, M., Polcher, J., 2020. Challenges for drought assessment in  
818 the Mediterranean region under future climate scenarios. *Earth-Science Reviews* 210, 103348.  
819 <https://doi.org/10.1016/j.earscirev.2020.103348>

- 820 Tritz, S., Guinot, V., Jourde, H., 2011. Modelling the behaviour of a karst system catchment using non-  
821 linear hysteretic conceptual model. *Journal of Hydrology* 397, 250–262.  
822 <https://doi.org/10.1016/j.jhydrol.2010.12.001>
- 823 Vautard, R., Kadygrov, N., Iles, C., Boberg, F., Buonomo, E., Bülow, K., Coppola, E., Corre, L.,  
824 Meijgaard, E. van, Nogherotto, R., Sandstad, M., Schwingshackl, C., Somot, S., Aalbers, E.,  
825 Christensen, O.B., Ciarlò, J.M., Demory, M.-E., Giorgi, F., Jacob, D., Jones, R.G., Keuler, K.,  
826 Kjellström, E., Lenderink, G., Levavasseur, G., Nikulin, G., Sillmann, J., Solidoro, C., Sørland,  
827 S.L., Steger, C., Teichmann, C., Warrach-Sagi, K., Wulfmeyer, V., 2020. Evaluation of the large  
828 EURO-CORDEX regional climate model ensemble. *Journal of Geophysical Research:*  
829 *Atmospheres* n/a. <https://doi.org/10.1029/2019JD032344>
- 830 Vörösmarty, C.J., Green, P., Salisbury, J., Lammers, R.B., 2000. Global Water Resources: Vulnerability  
831 from Climate Change and Population Growth. *Science* 289, 284–288.  
832 <https://doi.org/10.1126/science.289.5477.284>
- 833 Wada, Y., de Graaf, I.E.M., van Beek, L.P.H., 2016. High-resolution modeling of human and climate  
834 impacts on global water resources. *J. Adv. Model. Earth Syst.* 8, 735–763.  
835 <https://doi.org/10.1002/2015MS000618>
- 836 Zhao, S., Pereira, P., Wu, X., Zhou, J., Cao, J., Zhang, W., 2020. Global karst vegetation regime and its  
837 response to climate change and human activities. *Ecological Indicators* 113, 106208.  
838 <https://doi.org/10.1016/j.ecolind.2020.106208>
- 839